Understanding and evaluating the changing characteristics of Wind-driven rain loads in a warmer climate for Canada

Tarek Dukhan

Department of Civil Engineering and Applied Mechanics

McGill University, Montreal

November 2020

A thesis submitted to McGill University in partial fulfillment of the requirements of the degree of Master of Engineering.

ABSTRACT

The amount of rainfall that passes through a vertical plane, during the co-occurrence of rain and wind, is defined as Wind-driven rain (WDR). WDR is the most important moisture source affecting the performance of building façades, and can lead to several undesired results for buildings. In future, higher climate variability and more extreme events are expected. Therefore, Hygrothermal and durability analysis of façades require quantification of future WDR loads for a changing climate.

This study evaluates the changing characteristics of WDR loads across Canada for the end of century using an ensemble of regional climate model simulations for the Representative Concentration Pathway 8.5 emissions scenario. The regional climate model, i.e. the Global Environmental Multiscale model, is validated by comparing model-simulated WDR-related climate variables with observations and reanalysis products. The validation results provide confidence in using the model to assess the projected changes to WDR loads for Canada, albeit some biases.

Three types of WDR loads, based on semi-empirical equations, are considered in this study: (1) omnidirectional WDR, (2) directional WDR and (3) WDR spells. Omnidirectional and directional WDR amounts are calculated over periods of interest. The former indicates WDR exposure of a specific region, while the latter represents the potential moisture content of absorbent surfaces since it takes into account the façade orientation and wind direction. The WDR spell amounts are representative of the probability of rain penetration through the façade and more critical for design purposes. Furthermore, 3-year return levels of annual maximum WDR spell loads are also used to develop WDR risk category maps for Canada and specifically for 16 Canadian cities.

Future projections suggest large increases in WDR loads for some regions of Canada. The increases in these loads are mainly due to increases in both rainfall and wind magnitudes for Arctic Canada, while for other regions it is mostly due to changes in rainfall. Results indicate a shift in the timing of the highest monthly WDR loads from summer to fall. This suggests higher WDR penetration through wall systems, given the relatively low evaporation rate in fall compared to summer even in a warmer climate. Detailed city-level analysis of directional WDR loads suggests large increases for the most critical façade orientations for most of the sixteen cities considered, with the largest increases for those along the east and west coast. The projected changes to the characteristics of future WDR spells imply more severe extreme WDR events and higher deterioration risk. Furthermore, the developed WDR risk category maps help identify façade orientations with elevated risk in future climate which is crucial for the development of detailed guidelines to ensure climate-resilient buildings.

RESUME

La *pluie poussée par le vent* (PPPV) est définie comme étant la quantité de pluie qui passe par un plan vertical, lors de l'occurrence simultanée de pluie et de vent. La PPPV est la source d'humidité la plus importante affectant la performance des façades des bâtiments et peut mener à plusieurs effets indésirables au niveau des bâtiments. Dans le futur, une variabilité climatique plus élevée et des événements extrêmes sont attendus. Par conséquent, les analyses hygrothermiques et de durabilité des façades nécessitent une quantification des futures charges de PPPV qui auront lieu dans un climat changeant.

Cette thèse évalue les caractéristiques changeantes des charges de PPPV à travers le Canada pour la fin du XXIe siècle à l'aide d'un ensemble de simulations produites par un modèle climatique régional pour le scénario d'émissions de la voie de concentration représentatives 8.5 (*Representative Concentration Pathway 8.5*). La validation du modèle climatique régional utilisé (GEM - *Global Environmental Multiscale*) a été effectuée en comparant les variables climatiques reliées à la PPPV simulées par le modèle à des observations et des produits de réanalyse. Les résultats obtenus démontrent la validité de l'utilisation du modèle dans l'évaluation des changements projetés des charges de PPPV au Canada, malgré certains biais.

Trois types de charges de PPPV basés sur des équations semi-empiriques sont considérés dans cette étude: (1) PPPV omnidirectionnelle, (2) PPPV directionnelle et (3) les PPPV d'épisodes pluvieux. Les quantités PPPV omnidirectionnelle et directionnelle sont calculées pour des périodes d'intérêt. Le premier type indique l'exposition à la PPPV d'une région spécifique, tandis que le second représente la teneur en humidité potentielle des surfaces absorbantes car il prend en compte l'orientation de la façade et la direction du vent. Les quantités de PPPV d'épisodes pluvieux sont représentatifs de la probabilité de pénétration de la pluie à travers la façade et sont plus critiques à des fins de conception. De plus, les niveaux de retour sur 3 ans

des charges de PPPV d’épisodes pluvieux maximales annuelles sont également utilisées pour élaborer des cartes des catégories de risque associé à la PPPV pour le Canada et plus particulièrement pour 16 villes canadiennes.

Les projections futures suggèrent de fortes augmentations des charges de PPPV pour certaines régions du Canada. Les augmentations de ces charges sont principalement attribuables à l'augmentation des pluies et des vents dans l'Arctique canadien, tandis que dans d'autres régions, elles sont principalement attribuables aux variations des pluies. Les résultats indiquent un décalage de l’occurrence des charges mensuelles les plus élevées de PPPV de l'été vers l'automne. Cela suggère une pénétration plus élevée de la PPPV à travers les systèmes muraux, étant donné le taux d'évaporation relativement faible à l'automne par rapport à l'été, même dans un climat plus chaud. Une analyse détaillée à l’échelle urbaine des charges directionnelles de PPPV suggère de fortes augmentations pour les orientations de façade les plus critiques, dans la plupart des seize villes considérées, avec les plus fortes augmentations pour celles situées le long des côtes est et ouest. Les changements projetés des caractéristiques des futurs PPPV d’épisodes pluvieux impliquent des événements de PPPV extrêmes plus graves et un risque de détérioration plus élevé. En outre, les cartes des catégories de risque associé à la PPPV développées aident à identifier les orientations de façade présentant un risque élevé dans le climat futur, ce qui est crucial pour le développement de lignes directrices détaillées pour garantir la résilience des bâtiments au climat.

ACKNOWLEDGEMENTS

I would like to express my sincere gratitude to my supervisor, Prof. Laxmi Sushama for giving me the opportunity to conduct my Master's degree under her guidance and supervision. I would like to thank Prof. Laxmi Sushama for her continuous guidance, encouragement, motivation and support me during the course of this work. I would like to thank Prof. Laxmi Sushama for her tremendous effort in advising me, assistance with the interpretation of the results and financial support throughout this research.

I extend my gratitude to my lab colleagues, Bernardo Teufel, Katherine Zhao, Seok-Geun Oh, Caio Ruman, Vincent Poitras, Ju Liang and Luis Duarte for the many useful discussions we had, their assistance in preparing and extracting the data, and their valuable advice and incisive comments that made my work much easier. Special thanks to Vincent Poitras for the translation of my abstract.

I would like to thank my friends and CEGSS members for their company, friendship and motivation that helped me overcome the difficulties throughout my studies. Thanks to all the professors and staff members of the department of civil engineering and applied mechanics at McGill for their guidance. Finally, I would like to thank my family for their endless support. All of this would not have been possible without their unconditional support and continuous encouragement.

CONTRIBUTION OF AUTHORS

This thesis has been written following the requirements of Graduate and Postdoctoral Studies for a manuscript-based thesis. The main findings of the research undertaken by the author as part of his master's program are presented in a single manuscript. The author carried out the numerical analysis and wrote the manuscript under the supervision of Prof. Laxmi Sushama, his thesis supervisor. The publication detail is presented below:

- Dukhan, T. and Sushama, L. 2020. Understanding and modelling future wind-driven rain loads on building envelopes for Canada (Submitted to the 'Building and Environment' journal).

TABLE ON CONTENTS

LIST OF FIGURES

LIST OF TABLES

CHAPTER 1 INTRODUCTION

1.1 Background

The main function of building envelopes is to protect the occupied space from exterior environmental loads. Architectural aesthetics, energy efficiency, weather resistance, and durability of buildings depend on the performance of building façades. Wind-driven rain (WDR), which is rain that falls obliquely with the force of wind, can adversely affect the durability and hygrothermal performance of building façades. Therefore, better quantitative knowledge on WDR loads and their characteristics is an essential requirement for designing building façades with enhanced performance. However, quantifying impinging WDR on building envelopes is complex since it can be influenced by a number of parameters such as: wind speed, wind direction, horizontal rainfall intensity, raindrop size, building detailing, topology and the position on building façade (Blocken and Carmeliet, 2004). Several methods have been developed to quantify WDR loads, which fall under the following three main categories: (1) experimental, (2) semi-empirical and (3) numerical methods.

Various physical processes occur during and after the impact of raindrop on building façades. Apart from being lost by splashing, bouncing and evaporation, WDR can spread along the surface, adhere to the wall surface, or it can be absorbed if the surface material is porous (Fig. 1.1). Therefore, WDR loads on building envelopes is detrimental in that it can lead to mold growth, rain penetration, frost damage, discoloration by efflorescence, structural cracking, as well as appearance of surface soiling patterns on building façades (Straube and Burnett, 1997; Blocken and Carmeliet, 2004; Erkal et al., 2012).

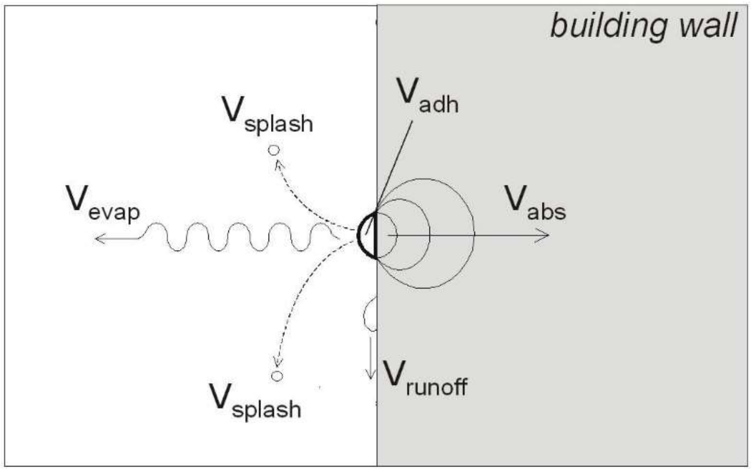

Figure 1.1 Representation of the physical processes that occur during and after impact of WDR at the building façade (Blocken and Carmeliet, 2012).

1.2 Motivation

WDR loads are much more critical than some of the other exterior environmental loads for building envelopes in most cases (Karagiozis et al., 2003), and therefore choosing appropriate building envelope to avoid the WDR-related negative effects is key. Understanding and quantifying WDR loads are crucial to develop better design standards and guidelines that help minimize moisture related damage and deterioration of building envelopes. The WDR loads in a future warmer climate can be different from that for current climate given projected increases in the intensity and duration of extreme events and increased climate variability in general (IPCC, 2013). According to Canada's changing climate report, increases in the intensity and duration of rainfall events for several regions are expected (Bush and Lemmen, 2019). The changes to the WDR related climate variables can lead to higher WDR exposure, and consequently pose bigger threats to the built environment. Thus, this research aims to evaluate future WDR loads and their characteristics in the context of a changing climate for the end of the 21st century for Canada, which will inform the development of detailed guidelines for climate-resilient buildings.

1.3 Research Objectives

The main purpose of this study is to explore future wind-driven rain loads on building façades and their characteristics in a warmer climate using transient climate change simulations of the limited area version of the Global Environmental Multiscale (GEM) model for the Representative Concentration Pathway (RCP) 8.5 emission scenario. The selected region of study is Canada. More specifically, this study:

- Conducts a literature review of established methods used in estimating WDR, particularly in the context of cold regions;
- Validates the regional climate model's capability in producing WDR-related climatic fields and derived WDR loads realistically over Canada using global reanalysis and station observations (Table A.1);
- Investigates projected changes to directional WDR loads and WDR spell load characteristics regionally and locally;
- Evaluates projected changes to WDR spell characteristics on the most critical façade orientation for 16 cities;
- Develops risk category maps (sheltered, moderate, severe and very severe), based on 3-year return levels of WDR spell loads;
- Draws conclusions on future WDR loads and characteristics which can inform the development of detailed climate change-informed design guidelines for building façades.

1.4 Thesis outline

The thesis herein is divided into four chapters. A general overview discussing the background, motivations, and objectives of this research is presented in the initial sections of Chapter 1. Chapter 2 reviews the existing literature surrounding the quantification of WDR loads and previous studies related to climate change impacts on these loads. Chapter 3 is drawn from a journal paper, which analyzes the characteristics of WDR in a future warmer climate. Finally, Chapter 4 presents the summary of the findings and suggestions for future relevant studies. Limitations of this research are also included in Chapter 4.

CHAPTER 2 LITERATURE REVIEW

2.1 Introduction

Impacts of WDR loads on building façades over time can be detrimental. Many examples of WDR-related damages and deterioration of buildings can be found in literature. For instance, Briggen et al. (2009) reported severe moisture damage (cracking, efflorescence, and rain penetration and discoloration) to the tower of a monumental building in the Netherlands due to WDR (Fig. 2.1). Likewise, Van den Brande et al. (2013) documented WDR-related damages to building façades in Belgium.

Figure 2.1 (a) Hunting Lodge St. Hubertus in the Netherlands and (b–e) moisture damage at the tower due to wind-driven rain: (b) salt efflorescence; (c) cracking due to salt crystallization; (d) rain penetration and discoloration; (e) cracking at inside surface (Briggen et al., 2009).

Several studies have focussed on estimating WDR load characteristics to mitigate their effects on building envelopes. These studies fall under the two following categories: (1) assessment of impinging WDR loads on building façades, and (2) study of the response of building components to these loads. Greater attention was attributed to the study of the former in the last decades compared to the latter (Blocken and Carmeliet, 2012; Blocken et al., 2013), which are discussed in the sections to follow.

2.2 Quantification of WDR loads

2.2.1 Experimental Methods

As stated in section 1.1, three main methods are used to quantify WDR loads on building envelopes. The experimental methods using field measurements and laboratory experiments provide basic knowledge on these loads. Measurements provide the basis of developing semi-empirical equations, and they are also necessary for validating the numerical simulations (Blocken and Carmeliet, 2005). However, there are many drawbacks of experimental methods as measurements are time-consuming, difficult, expensive and susceptible to errors (Hogberg et al., 1999; Blocken and Carmeliet, 2004). They also provide limited spatial and temporal information, and the application of measurements at a specific site to other locations is limited. Blocken and Carmeliet (2006b) carried out a study to investigate the errors associated with WDR measurements, and found that evaporation, splashing of drops, condensation on the collective area and wind errors are the main sources for error involved in measurements. WDR experimental studies conducted in the Canadian context include Ge and Krpan (2009), and Nath et al. (2015), among others. Ge and Krpan (2009), from their experimental study carried out to assess WDR exposure on eight buildings in British Colombia, reported that WDR exposure is significantly influenced by local topography and surroundings as well as building geometry and details. Moreover, Nath et al. (2015) conducted measurements on three buildings in three different Canadian regions (i.e. Fredericton, Montreal and Vancouver) to quantify and explore the spatial distribution of WDR loads on building façades. The results were then compared to predicted values based on a semi-empirical model. WDR was found to vary along both the building height and width, unlike the model's suggestion of no change in WDR across the width of the building.

2.2.3 Semi-empirical equations

Databases of WDR field measurements are not commonly available since WDR is not one of the standard meteorological variables measured at weather stations. WDR is also characterised by high spatial and temporal variabilities (Nore et al., 2007). This has encouraged researchers to develop semi-empirical relationships between WDR quantity and the influencing climate variables. First, a qualitative approach using the concept of WDR index, which is the product of mean annual wind speed and total horizontal rainfall amount, was adopted. This index was used to develop WDR maps for different countries (Blocken and Carmeliet, 2004). For instance, Boyd (1963) constructed a WDR map for Canada based on observational records of more than 10 years within the 1931–1960 period obtained from 141 stations (Fig. 2.2).

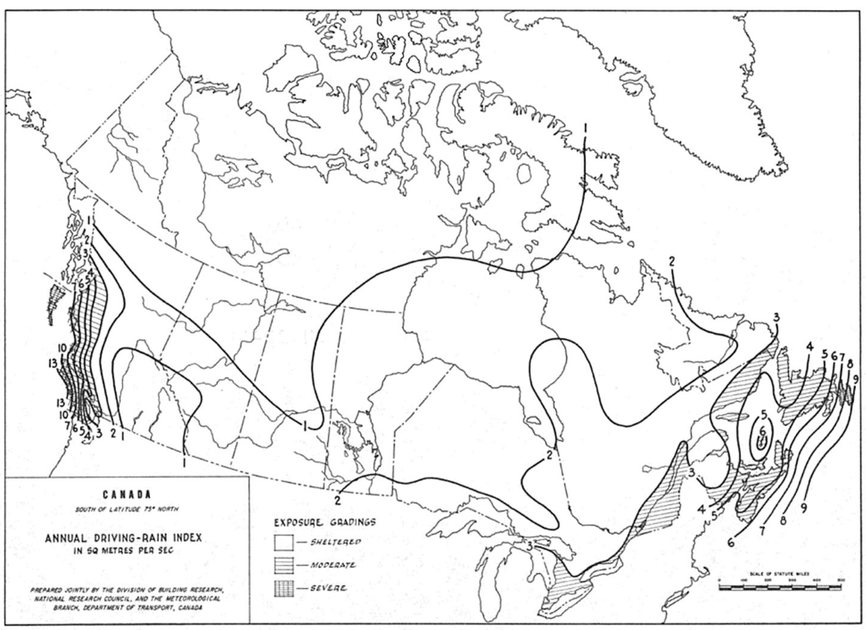

Figure 2.2 Annual Driving-rain index for Canada (Boyd, 1963).

Hoppestad (1955) developed Eq. (2.1) to determine the intensity of WDR passing through an imaginary vertical surface (R_{WDR}):

$$R_{WDR} = k \cdot U \cdot R_h \ . \tag{2.1}$$

Here, U is the wind speed, R_h is the horizontal rainfall intensity and k is the WDR coefficient. Average values for WDR coefficient were obtained for 4 different locations yielding an average value of 0.180. It is pertinent to mention that the wind direction in this equation is assumed to be always perpendicular to the surface. Lacy (1965) amended Eq. (2.1) by using empirical relationships of median raindrop size as:

$$R_{WDR} = 0.222 \cdot U \cdot {R_h}^{0.88} \cong \ 0.222\ U \ . R_h \ . \tag{2.2}$$

The above studies and equations formed the base for all semi-empirical models that were later developed, informed by considerable amount of field measurements. The recent models provide factors to account for the difference between airfield conditions and WDR deposition on certain building façades. The most commonly used models are: (1) The Straube and Burnett model (Straube and Burnett, 2000), (2) The ASHRAE 160 model (ASHRAE, 2009) and (3) The ISO Standard 15927 (ISO, 2009).

Straube and Burnett (2000) proposed the driving rain factor (DRF) which is equal to the inverse of the terminal drop velocity. This led to express WDR as the following equation:

$$R_{WDR} = DRF \cdot \ V(z) \ \cdot \ R_h \ \cdot \ \cos{(\theta)} \ , \tag{2.3}$$

where $V(z)$ is the wind speed at the height of interest (z), R_h is the rainfall rate on a horizontal plane and θ is the angle between the wind direction and the line normal to the surface (Note: $\cos{(\theta)}$ is equal to 1 for airfield WDR, assuming the wind is perpendicular to the surface at all the time). The driving rain factor (DRF) depends on the raindrop size as well as the storm type. Straube and Schumacher (2006) provided a detailed procedure for estimating this factor using the median raindrop size since there is a range of raindrop sizes associated with any storm.

Experimental work and measurements by Straube (1998) validated the proposed equation and found that the quantity of WDR loads can be estimated with a better accuracy (Fig. 2.3).

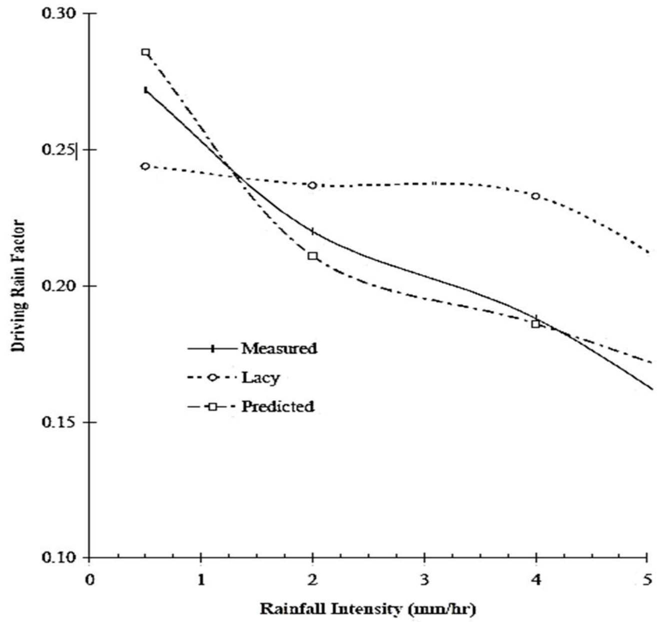

Figure 2.3 Comparison of measured DRF with that calculated by Lacy's method (Straube, 1998).

It is important to note that the equation above (Eq. 2.3) estimates the airfield WDR in an undisturbed region. However, this model introduced the rain deposition factor (RDF), which considers the effect of building shape and size, to transform free WDR to the rate or rain deposition on building façades. This model also uses correction factors to account for onsite conditions. These factors are the Exposure and Height Factor (EHF) and Topography Factor (TOF). Therefore, the amount of WDR deposited on a particular spot on a building façade with a specific orientation in a particular location is given as:

$$R_{WDR} = RDF \cdot DRF \cdot \ V(z) \cdot \ R_h \ \cdot \cos(\theta) \cdot EHE \cdot TOF \ , \qquad (2.4)$$

Additional information about the factors and their values can be found in Straube and Burnett (2000).

The ASHRAE 160 proposed a similar equation to assess the WDR hitting a vertical surface (R_{WDR}) as follows:

$$R_{WDR} = 0.2 \cdot F_E \cdot F_D \cdot U_{10} \cdot \cos(\theta) \cdot R_h \,, \qquad (2.5)$$

where F_E and F_D represent the rain exposure factor and the rain deposition factor, respectively. In this model, the hourly wind speed at 10 m height (U_{10}) and a constant WDR coefficient (0.2) are used. The exposure factor is governed by the building height and terrain type, while the deposition factor depends on the wall type.

In the ISO standards, two quantities are provided to assess WDR: (1) annual airfield WDR index and (2) airfield WDR spell index (ISO, 2009). The former index affects the moisture content of the absorbent surfaces, while the latter influences the rain penetration through the building façades and joints. For both indices, it is recommended to use hourly data of wind and rainfall for at least 10 years. The annual airfield WDR index is used to quantify WDR over a period of interest and it is given as:

$$I_A = \frac{2}{9} \frac{\sum v\, r^{8/9} \cos(\mathrm{D}-\Theta)}{N} \,, \qquad (2.6)$$

where v represents hourly mean wind speed, r is the total hourly rainfall, N is the number of years of available data, and D is hourly the wind direction from north and Θ is the wall orientation relative to north. For this index, the summation is taken for all hours in the studied period when the wind is blowing against the wall (i.e. $(D - \Theta)$ is positive).

Spell index, which evaluates WDR loads during a spell event, is also available in literature. A WDR spell can be defined as the period of WDR exposure in which the risk of rain penetration increases since the input of water exceeds the loss by evaporation. The drying period that separates consecutive spells depends on the type of wall system or openings in which rain penetration would occur (Fig. A.1). The ISO standard proposes that the drying period should last at least 96 hrs with no WDR hitting the surface for masonry walls, while it does not provide guidelines for the length of this period for other wall systems and openings. To calculate the WDR spell index, the following term is computed for each spell within the period of available data as follows:

$$I'_S = \frac{2}{9} \sum v \, r^{8/9} \cos(\mathrm{D} - \Theta), \qquad (2.7)$$

where the summation is taken over all hours of the spells for which the wind is blowing against the wall. The 67th percentile is calculated using the I'_S values of all spells during the considered years. This percentile value defines the WDR airfield spell index (I_S), and it represents the maximum value of spell load likely to occur once every three years. However, a study conducted by Orr and Viles (2018) found that the ISO method underestimates the worst WDR spell possible to occur in any given three-year period when compared to results obtained from a method based on extreme value analysis. This can be mainly attributed to incorporating percentiles in the used protocol.

The ISO airfield indices above represent the amount of WDR collected by a free standing driving rain gauge in flat open terrain. However, the ISO model also provides coefficients to convert the airfield indices to wall indices in order to estimate the amount of rain that would impact on a real wall. These coefficients include the terrain roughness coefficient (CR), the topography coefficient (CT), the obstruction factor (O), and the wall factor (W). More details about these coefficients are available in ISO (2009).

Several studies have been conducted to quantify WDR for different countries using these models. For instance, Straube and Schumacher (2006) quantified WDR loads for 18 Canadian cities using combined hourly weather data from different sources for the 1965-1989 period (Fig. 2.4). Pérez-Bella et al. (2012) produced a map of WDR exposure for Spain based on weather data from 80 stations located throughout the country. In these studies, WDR calculations are based on airfield conditions which indicate the WDR exposure at a given region.

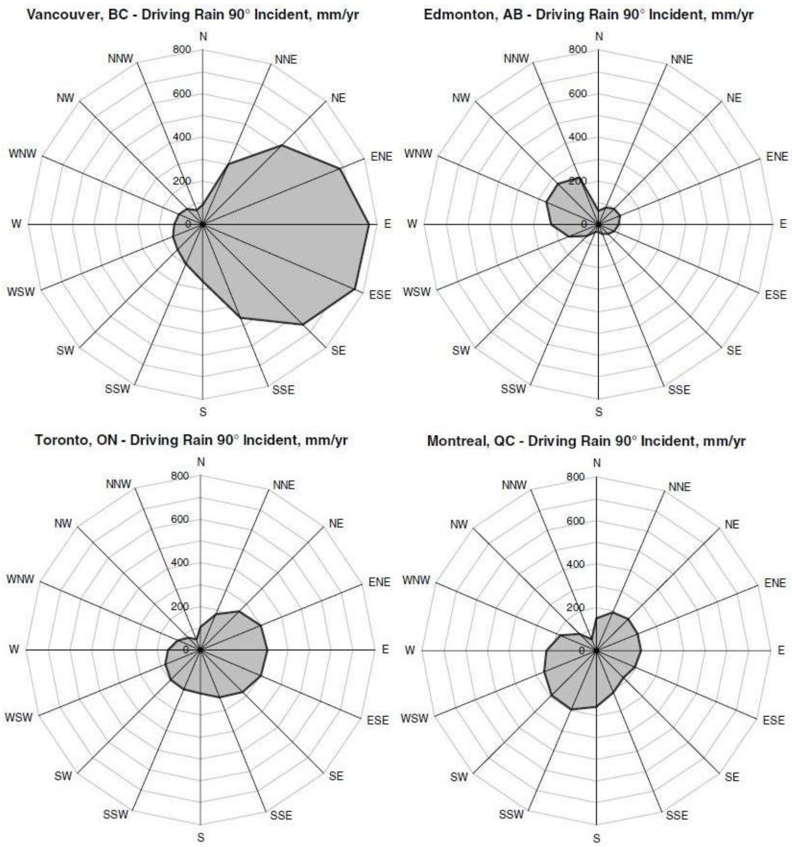

Figure 2.4 Directional WDR plots for Vancouver, Edmonton, Toronto and Montreal (Straube and Schumacher, 2006).

Furthermore, a number of studies evaluated the ability of semi-empirical model of estimating WDR deposition on building façades. Blocken et al. (2011) found that the estimated values of WDR on specific façade can show large discrepancies which is mainly attributed to wind-blocking effect which refers to decreased WDR exposure due to the presence of the building and the associated wind speed slow-down near the surface. Also, they found that Straube and Burnett model overestimates WDR on vertical and top edges of buildings. Nath et al. (2015) found that ISO model can overestimate WDR on façades due to the lack of correction factors for different building geometries. Kubilay et al. (2014a) concluded that the existing semi-empirical models give limited information on WDR distribution on building façades. Overall, semi-empirical models are simple and easy to use, but they are limited to simple building geometries. Therefore, the capabilities and deficiencies should be taken into account when estimating WDR deposition on facades using these models (Blocken et al., 2011).

2.2.3 Numerical methods

The drawbacks of using experimental and semi-empirical methods drove researchers to employ numerical analysis for further investigations. The pioneering work by Choi in the 1990s have been the leading foundation of numerical methods and computational fluid dynamic (CFD) modeling in WDR research (Blocken and Carmeliet, 2004). The numerical simulation technique in Choi (1993, 1994) combining the Reynolds-averaged Navier–Stokes (RANS) equations and a Lagrangian particle tracking (LPT) model allowed determination of the spatial distribution of WDR on building façades under steady-state conditions of wind and rain. The numerical simulation was further enhanced by adding a temporal component and including a new weighted data averaging technique allowing for the determination of both spatial and temporal WDR distribution (Blocken and Carmeliet, 2000a, 2000b). Huang and Li (2010) presented another approach based on Eulerian multiphase (EM) model for evaluating WDR on building envelopes which simplifies the evaluation of WDR parameters and the boundary condition treatments.

Studies that compared CFD model results with measurement data showed that the numerical models can provide accurate results of WDR distribution on façades (Blocken and Carmeliet, 2007; Abuku et al., 2009a; Huang and Li, 2010; Blocken et al., 2011; Kubilay et al., 2014b). Although detailed inputs of building geometries and surrounding topology are required for performing the numerical simulations, CFD modelling is essential to understand WDR load distribution on buildings, particularly buildings which have detailed façades (i.e. heritage buildings). Additionally, Numerical methods can contribute to the further advancement and development of the semi-empirical models.

2.3 Interaction of WDR and building façades

As mentioned earlier, WDR is influenced by the raindrop size as well as other climatic parameters. Rychtáriková and Vargová (2008) carried out a study to explore the raindrop trajectories for 17 different raindrop sizes ranging from 0.3 mm to 6 mm and for 8 different wind-flow patterns with different wind speeds. They found that, in general, trajectories are more inclined and distorted for smaller raindrops and higher wind speeds, while they tend to be more linear for large drops and lower wind speeds (Fig. 2.5). In their study, self-protecting features of buildings such as overhangs were found to reduce the deposition of WDR on building façades. Similar results were found in Ge and Krpan (2009) as lower catch ratios have been observed for façades with overhangs.

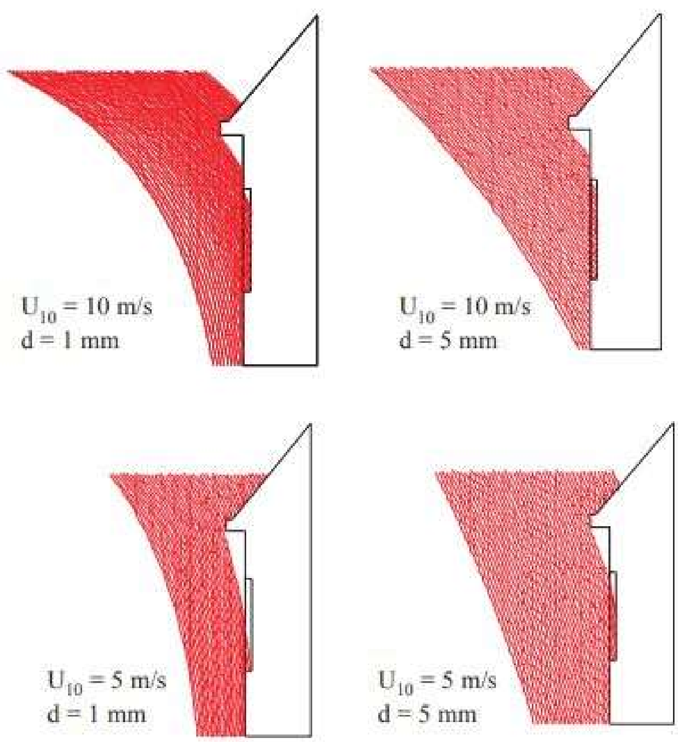

Figure 2.5 Example of raindrop trajectories for raindrop diameters d = 1 and d = 5 mm in the wind speed U10 = 10 m/s and 5 m/s (Rychtáriková and Vargová, 2008).

Foroushani et al. (2014) further investigated the effect of overhangs on WDR using CFD-based numerical simulations. They concluded that overhangs provide protection, particularly for the immediate parts below the overhangs, due to two effects. The direct effect is that overhangs provide shade and the indirect effect is due to the disturbance to the incoming wind created by overhangs. As the width of overhang increases, both direct and indirect effects increase. This leads to more efficient performance of overhangs in reducing the impact of WDR on buildings. Moreover, Ge et al. (2017) used a six-storey building located in Vancouver and equipped with retractable overhang to evaluate the effect of overhangs on WDR loads experimentally by comparing the spatial distribution of these loads on the façade with and without the overhang. They found that the overhang significantly reduced WDR loads on this building. The protection provided by the overhang was found to increase from the side edges to the center of the façade. They also concluded that the effectiveness of overhangs in reducing WDR depends on the climate variables as it increases for lower wind speeds and for oblique winds.

Moreover, there are several other characteristics of buildings that can also influence WDR. Blocken and Carmeliet (2006a) found that the "wind-blocking effect", which refers to the disturbance of wind-flow pattern and the associated decreased wind speed near the surface due to the presence of the building, is one of the main factors that govern WDR distribution on façades, particularly for isolated buildings. This effect causes lower WDR exposure for both the top corners and lower parts of building façades. They also found that wind-blocking effect increases for larger dimensions (i.e. Length and height) of building façades. This illustrates and justifies why isolated high-rise buildings do not necessarily receive more WDR on their façades compared to isolated low-rise buildings. However, given the situation of a typical city where there are many low-rise buildings with only a few high-rise buildings, low-rise buildings are normally sheltered by surrounding buildings and high-rise buildings are not substantially sheltered (Blocken et al., 2013). Hence, the façades of high-rise buildings are relatively exposed to more WDR. Furthermore, Kubilay et al. (2017) analyzed the influence of façade details on WDR exposure on building facades using CFD based model for WDR on a stand-alone mid-rise residential building. Results showed that even a very small surface detail, such as a windowsill with a size of 0.10 m, can have large impact on WDR exposure on a building.

Many studies recently focussed on investigating and understanding the response of building façades to WDR loads and their effects on the hygrothermal performance of building envelopes. Hens (2010) presented three case studies to address what happens when raindrops strike a surface using actual Heat, Air and Moisture (HAM) models. In this study, the effects of absorbed rainwater in wall assemblies were estimated reasonably well using the actual HAM tools, while the problems caused by runoff were not addressed using the actual model due to the complexity presented. However, a simplified numerical model for rainwater runoff on building façades is presented in Blocken and Carmeliet (2012). This model can be considered as a supplement to the existing building envelope HAM models in spite of its limitations and simplifications. Van den Brande et al. (2013) presented the implementation and application of a rainwater runoff model coupled to a 2D HAM model. They found that runoff of WDR can have significant influence on the moisture behaviour of the façade. For instance, facades of materials with low capillary absorption coefficients can absorb twice the amount of impinging WDR when runoff is included.

Moreover, Abuku et al. (2009b) analyzed the impacts of WDR on the hygrothermal behaviour of historic brick wall buildings in a cold and humid climate. This study demonstrated the large impact of WDR on mold growth, and reported increases in indoor relative humidity and energy consumption for heating due to WDR loads. Erkal et al. (2012) evaluated the WDR impact performance of different porous masonry materials for different raindrop diameters, impact speeds and impact angles. They found that WDR can cause surface erosion and detachment of materials from masonry walls. The assessment of surface erosion and resulted wetting showed that unfired clay bricks experience relatively higher erosion due to their low bond strength, and solid hand-cut historic clay bricks were wetted more due to their high permeability. Furthermore, a study was conducted to further explore the response of masonry walls to WDR by Cacciotti (2020), found that rain penetration can induce durability problems, degradation in mechanical properties, stress redistribution and lowering of damage and failure stresses in bricks. It was also found that the combined damaging effect of moisture-induced degradation and additional adverse conditions, such as temperature and salt actions, can induce structural damage risks.

2.4 Climate change and WDR

2.4.1 Reginal climate models

Studies conducted to assess the impacts of climate change and its applications to vulnerability and adaptation assessments require future projections. Global climate models can describe the large-scale climate features effectively, such as general circulation of the atmosphere and oceans (Rummukainen, 2010). However, it is difficult to capture regional and local climate aspects using relatively coarse GCMs. In addition, high resolution GCMs require high computational resources. Therefore, regional climate models (RCMs)were developed by downscaling climate fields produced by GCMs to bridge the gap from large scale climate fields to smaller scales which are required for assessing climate change impacts through the use of a limited area physically-based model (i.e. Dynamical downscaling). RCMs are driven by transient boundary conditions obtained from GCMs at the lateral boundary. RCMs account for the sub-GCM grid scale forcing and physical processes such as complex topography, coastlines, inland bodies of water and land cover distribution (Giorgi, 2019).

RCMs can suffer from biases imposed at their lateral boundaries (Armstrong et al., 2019). To evaluate the performance of RCMs with reduced systematic biases, an experiment called "perfect boundary conditions" can be performed (Rummukainen, 2010; Giorgi, 2019). In this experiment, RCMs are driven by global reanalyses (e.g. ERA-Interim and ERA5) and a comparison is undertaken with the observational datasets which enables evaluating the performance of the model. In This research, the model used is the limited area version of global environment multiscale (GEM) model and the experimental domain covers the pan-Arctic region.

2.4.2 Studies on WDR and climate change

Assessment of future WDR is crucial to develop guidelines and standards that minimize WDR exposure and associated impacts on building façades. In 2011, the Building Standards Division of Scottish Government evaluated the need for new guidance on WDR based on climate data for the 1991–2011 period (Reid and Garvin, 2011). Although increases to rainfall intensity were observed over this period, changes were not considered significant to render the existing standards irrelevant in the short term. For Finland, Pakkala et al. (2016) analyzed future WDR loads for four locations based on the airfield annual WDR index for the end of the century. They found that all locations will experience increases in WDR in the range of 31% to 54%. Orr et al. (2018) evaluated the changes to WDR spells and exposure for eight sites in UK under high emission scenario by using probabilistic generation of hourly data. In this study, assessment of annual and seasonal WDR exposure as well as spell index were included. The results suggested higher volumes of WDR spells for shorter durations which imply higher possibility of building element failure.

Nik et al. (2015) investigated the prospective impacts of climate change on WDR loads and their effects on the hygrothermal performance of common wall constructions in Gothenburg, Sweden. In this study, several regional climate model (RCM) datasets were applied in a HAM tool to analyze the transient coupled heat and moisture transport in multi-layer façade. This allowed to run long-term hygrothermal simulations of building components. They found that higher amount of moisture is expected to accumulate in walls in the future.

2.5 Knowledge gap and Conclusions

The study of WDR and its impacts on building envelopes is a growing field of research particularly in the context of a changing climate, given the need to minimize moisture related problems in the future. A few studies have looked at the impacts of climate change on WDR loads, particularly for Sweden, Finland and UK. However, evaluation of future WDR loads, which is essential to develop design guidelines for climate-resilient buildings, is lacking for Canada. This thesis addresses this knowledge gap and provides detailed analysis of projected changes to WDR using the limited version of global environment multiscale (GEM) model which has been applied extensively to study climate and climate change impacts (Jeong and Sushama, 2019; Teufel et al., 2019; Oh and Sushama, 2020; Zhao and Sushama, 2020). A five-member transient climate change simulation ensemble is used to better quantify uncertainties (Fig. A.2). Another GEM simulation driven by ERA-Interim is used to evaluate the boundary forcing errors.

Given the regional and city level focus in this study, and supported by literature review, it was decided to use semi-empirical models to estimate WDR loads and related characteristics. Building-level studies would require CFD modelling, which is outside the scope of this research, but will be useful to consider in future research. The semi-empirical model selected for this study is the Straube and Burnett model (2000) as it has been applied over Canada and validated with WDR measurements (Straube, 1998; Straube and Burnett, 2000). Detailed information about the models used along with the results are presented in Chapter 3.

Chapter 3 Understanding and modeling future Wind-driven Rain loads on building envelopes for Canada

Tarek Dukhan[1*], Laxmi Sushama[1]

[1] Department of Civil Engineering and Applied Mechanics, Trottier Institute for Sustainability in Engineering and Design, McGill University, Montreal, QC, Canada

*Corresponding author E-mail: tarek.dukhan@mail.mcgill.ca

Abstract

Wind-driven rain (WDR) is the amount of rainfall that passes through a vertical plane due to its co-occurrence with wind, which can adversely impact the performance of building façades. Hygrothermal and durability analysis of facades require quantification of future WDR loads for a changing climate. This study evaluates projected changes to WDR loads across Canada for the end of century regional climate model simulations for the Representative Concentration Pathway scenario 8.5. WDR loads are quantified in terms of omnidirectional and directional WDR amounts over periods of interest, which are relative indicators of WDR exposure and potential moisture content of absorbent surfaces, respectively. Furthermore, return levels of annual maximum WDR spell amounts, which are representative of the risk penetration through the façade, are also used to develop WDR risk category maps for Canada and specifically for 16 Canadian cities.

Future projections suggest increases in WDR loads for Arctic Canada, due to increases in both rainfall and wind magnitudes, while for other regions with increased loads, it is mostly due to increases in rainfall. Results suggest a shift in the timing of the highest monthly WDR loads from summer to fall, which is suggestive of higher WDR penetration through wall systems, given the relatively low evaporation rate in fall compared to summer even in a warmer climate. Furthermore, the developed WDR risk category maps show changes to critical façade

orientations with elevated risk in future climate. This information is crucial in the development of detailed guidelines to ensure climate-resilient buildings.

Keywords: wind-driven rain, building facades, wind-driven rain spells, climate change, regional climate modelling, risk categories.

3.1 Introduction

Wind-driven rain (WDR) is defined as the amount of rainfall that passes through a vertical plane due to its co-occurrence with wind. WDR studies are important and relevant for various fields such as earth sciences, meteorology and most importantly building science, where it is considered as one of the most significant sources of moisture affecting the durability and hygrothermal performance of building facades. WDR can lead to several undesired results for buildings such as mold growth at the interior wall surface, efflorescence, erosion of building materials, freeze-thaw damage, water penetration and surface soiling (Straube and Burnett, 1997; Blocken and Carmeliet, 2004). Therefore, quantifying WDR and understanding its characteristics, particularly in a changing climate, are essential to improve and establish better design standards for façades that can help minimize moisture related problems. WDR loads are also used as boundary conditions for Heat, Air and Moisture (HAM) transfer analysis of building components (Blocken and Carmeliet, 2000a).

Airfield WDR, which is the WDR that is not influenced by the presence of buildings or other obstructions, is governed by several meteorological parameters such as wind speed, wind direction, horizontal rainfall intensity, raindrop size, and rain event duration. Impinging WDR on building facade is more complicated since it is influenced by a large number of parameters such as environment topology, building geometry, façade detailing and all relevant meteorological parameters (Blocken and Carmeliet, 2004; Nore et al., 2007) Since wind and rainfall are highly variable in both space and time, WDR, both in free space and in deposited form on building façade, is also characterised by high spatial and temporal variabilities.

Several methods have been developed to quantify the impinging WDR on building façade. These methods can be divided into three main categories: (1) experimental methods (2) semi-empirical methods and (3) numerical simulations based on Computational Fluid Dynamics

(CFD) models. Though measurements of WDR by using WDR gauges have provided some basic knowledge, there are many drawbacks of using experimental methods. The measurements are difficult, time-consuming, and provide limited spatial and temporal information (Hogberg et al., 1999). On the other hand, semi-empirical relationships between WDR and relevant climatic parameters, developed based on experimental observations, are easy to use but they are limited to simple building geometries. Numerical methods can provide detailed information on the spatial distribution of WDR on complex building geometries. However, these methods are computationally expensive. Moreover, these methods also require a large amount of preparation work as detailed inputs of many building aspects and site geometries are often required. Consequently, it is challenging to use CFD modelling packages to quantify WDR for design purposes (Straube and Burnett, 2000).

According to the Fifth Assessment Report of the Intergovernmental Panel on Climate Change (IPCC, 2013), increases in climate variability and extreme events are expected in a future warmer climate. According to Canada's climate change report, increases in the intensity and duration of rainfall events are projected for several regions of Canada for different emission scenarios (Bush and Lemmen, 2019). As for wind, the climate change signal is less clear, except for northern Canada, where studies suggest increases in wind magnitude in future climate (Jeong and Sushama, 2019). These changes to wind and rainfall characteristics make the built environment more vulnerable to wind driven rain. Over the last several years, WDR has received increased attention. Many studies have been undertaken to investigate the characteristics of WDR loads (e.g. Straube and Schumacher (2006), Nik et al. (2015), Carbonez et al. (2015), Pakkala et al. (2016), and Orr et al. (2018)). However, studies that explore future changes to WDR loads in the context of a changing climate are lacking for Canada. Furthermore, systematic guidance on future WDR loads and associated thresholds are needed in the design standards and building codes of Canada.

The main purpose of this study therefore is to investigate climate change impacts on WDR loads for the 2071-2100 future period, with respect to the current 1981-2010 period over Canada using a 5-member transient climate change simulation ensemble of the limited area version of the Global Environmental Multiscale (GEM) model, corresponding to Representative Concentration Pathway (RCP) 8.5 scenario. This study also provides WDR risk category maps for different façade orientations, which can contribute to the development of detailed guidelines for climate-resilient buildings.

The rest of this chapter is organized as follows. Section 3.2 gives a brief description of the climate model and simulations used in this study, along with the datasets that are used to validate the model. In Section 3.3, the methods used to estimate WDR loads are elaborated. Section 3.4 provides validation of WDR-related climate variables and Section 3.5 focusses on projected changes to WDR loads across Canada. Finally, summary and conclusions are given in Section 3.6.

3.2 Climate model and observation data

3.2.1 Climate model

The regional climate model used in this study is the limited area version of the GEM model (Côté et al., 1998) that uses a non-hydrostatic dynamical core with a hybrid vertical coordinate. GEM employs semi-Lagrangian transport and a (quasi) fully implicit stepping scheme. More details about the model can be found in Diro and Sushama (2019). However, the physics parameterization is concisely described here. Convective processes are represented in the model following Kain and Fritsch (1992) and Bélair et al. (2005) for deep and shallow convections, respectively. The resolvable large-scale precipitation is computed following Sundqvist et al. (1989). Radiation is parametrized by Correlated K solar and terrestrial radiation of Li and Barker (2005). The planetary boundary layer scheme follows Benoit et al. (1989) and

Delage (1997), with some modifications as described in Zadra et al. (2012). The land surface scheme used in GEM is the Canadian Land Surface Scheme (CLASS) (Verseghy, 2009), which allows flexible soil layer configuration. Twenty-six layers are used in the simulations considered in this study, with layer depths varying non-linearly from 0.1 m to 5 m. Lakes, both resolved and sub-grid scale, are represented by the Flake model (Mironov et al., 2005; Mironov et al., 2010).

A five-member GEM transient climate change simulation ensemble spanning the 1950–2100 period is considered in this study. The simulations are performed over a pan-Arctic domain encompassing regions north of the 49th parallel and consists of 172×172 grid points at 0.5° resolution in the horizontal and 56 vertical levels with the model top near 10hPa. Each member of the GEM ensemble is driven at the lateral boundaries by a different member of a CanESM2 (Canadian Earth System Model, V2) initial condition ensemble corresponding to RCP8.5 scenario. The RCP8.5 scenario corresponds to the highest greenhouse gas emissions scenario and does not include any specific climate mitigation target, leading to a radiative forcing of 8.5 W/m^2 at the end of 21st century (Riahi et al., 2011). These CanESM2-driven GEM simulations will be referred to as GEM-CanESM2, hereafter. An additional GEM simulation driven at the lateral boundaries by ERA-Interim reanalysis provided by the European Center for Medium-Range Weather Forecast (ECMWF; (Dee et al., 2011), for the 1979-2016 period, referred to as GEM-ERAInterim, is also considered to validate model performance. Although the simulations are performed over a Pan-Arctic domain, the analysis presented in this chapter focusses over Canada (Fig. 3.1).

3.2.2 Observation data

For validating model simulated rainfall and wind, hourly values of the same variables from ERA5 (Hersbach and Dee, 2016; Hans et al., 2019) reanalysis at 0.25° resolution and 6-hourly values from ERA-Interim reanalysis (Dee et al., 2011) at 0.75° resolution for the 1981-2010 period are used. The comparison of GEM_ERAInterim with ERA-Interim reanalysis also provides the opportunity to assess the added value of downscaling ERA-Interim with GEM model. The Climatic Research Unit (CRU) dataset (Harris et al., 2020) is also used to validate rainfall. Point observations obtained from Environment and Climate Change Canada (ECCC) are also used to validate the directional distribution of wind speeds for the sixteen selected locations considered in this study (see Fig. 3.1).

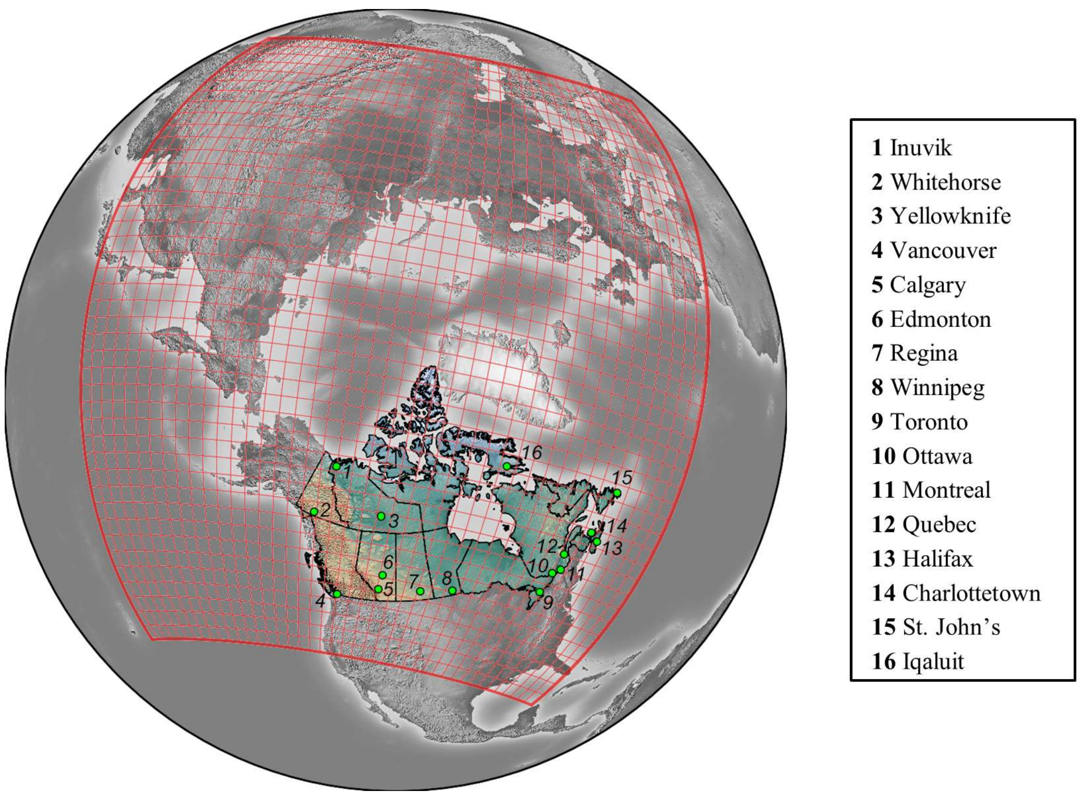

Figure 3.1 Model experimental domain, with the analysis region (Canada) shown in color. The 16 cities considered in this study are also shown.

3.3 Methodology

3.3.1 Definitions and approaches

Analysis and quantification of WDR can be performed and presented in various ways. Additionally, different definitions for WDR loads can be found in the literature. In this study, three types of WDR loads are discussed: (1) Omnidirectional airfield WDR load, which represents the cumulative WDR amounts during the period of interest (i.e., annual, seasonal or monthly); WDR amounts are estimated at 10 m height in an open airfield with no obstructions, and irrespective of the wind direction; (2) Directional WDR load, which is WDR deposited on a generic building façade with a specific orientation that takes into account the effect of the angle between the WDR direction and orientation of the façade; and (3) WDR spell amounts/loads deposited on a generic building façade, where a WDR spell is a continuous period of WDR resulting from consecutive rainfall events separated by short dry periods (details provided below). These three types of loads will hereafter be referred to as WDR1, WDR2 and WDR3, respectively.

The semi-empirical model proposed by Straube and Burnett (2000) is used to evaluate WDR1 and WDR2, while ISO Standard 15927-3 (2009) is used to estimate WDR3. WDR1 and WDR2 are relative indicators of WDR exposure and moisture content of absorbent surfaces, respectively, while WDR3 is more representative of the possibility of rain penetration through masonry walls or joints in different wall systems (ISO, 2009). Return levels of annual maximum WDR3 are further used to develop exposure risk category maps for different façade orientations following the BRE Report BR262 approach (BRE, 2002). Further details regarding the approaches to estimate the WDR loads are provided below.

3.3.1.1 Estimation of WDR1 and WDR2 loads

WDR loads depend on raindrop size, among other factors. Previous studies on WDR load estimation using empirical relations between raindrop size, rainfall intensity and wind speed are available in the literature. For example, Lacy (1965) proposed a simple equation relating wind speed and rainfall intensity to the airfield WDR. After additional investigations and a considerable amount of field measurements, a generalized and improved relationship was proposed by Straube and Burnett (2000). This relation/model is used to estimate WDR1 and WDR2 in this study as:

$$WDR1(2) = \sum_{i=1}^{t} DRF_i \times V_i \times Rh_i \times \cos(\theta)\ , \tag{3.1}$$

where V is the hourly wind speed at 10 m level, Rh is the hourly horizontal rainfall intensity and θ represents the angle between the wind direction and the normal vector of the facade of interest ($\theta = 0^o$ for WDR1) and DRF is the driving rain factor which can be calculated from the terminal drop velocity V_t as:

$$DRF = 1/V_t\ , \tag{3.2}$$

According to Dingle and Lee (1972), the terminal drop velocity can be related to the raindrop diameter ϕ as

$$V_t\ (\emptyset) = -\ 0.166033 + 4.91844\ \emptyset - 0.888016\ \emptyset^2 + 0.054888\ \emptyset^3\ , \tag{3.3}$$

Since there is a range of rain drop sizes associated with any rainfall event, the median raindrop diameter is used. It is calculated using the cumulative distribution function of the raindrop diameter as a function of rainfall intensity (Best, 1950) as:

$$F(\emptyset) = 1 - \exp\left(-\left(\frac{\emptyset}{1.3\ Rh^{\ 0.232}}\right)^{2.245}\right)\ , \tag{3.4}$$

The above relations were validated by Straube (1998) by comparing with field experiments. To estimate the exposure at a specific location on a given façade, additional factors that account for building geometry, topography and height, and upwind roughness must be considered.

3.3.1.2 Estimation of WDR3 loads and development of WDR exposure maps

The WDR spell as already defined is a period of consecutive rainfall events separated by short dry periods and can vary in length from one hour to several hours and days. In case of rain penetration through masonry, which requires a prolonged input of water, according to the ISO standards, it can take up to 96 hours for the evaporative loss to exceed the water gain from WDR loads. In this study we therefore consider the generic case of a masonry facade and use

96 hrs as the minimum duration of the dry period separating two WDR spells. In other words, the maximum duration of the dry period between consecutive rainfall events striking a certain facade (i.e. positive values of $cos\theta$) within a WDR spell should be less than 96 hrs. For rain penetration through doors, windows and other similar openings in the facade, shorter-term and more intense WDR under high pressure difference (driving rain wind pressure) should be considered.

In this study, 3-year return levels of annual maximum WDR3 ($\mathrm{WDR3_3}$ hereafter), which is estimated through extreme value analysis using the Gumbel distribution (Viessmann et al., 1977) is used following Orr and Viles (2018). This approach is equivalent to the initial recommendation of ISO to consider the 67th percentile of WDR3, but it overcomes to some extent the drawbacks associated with small WDR3 sample size for some locations, which can lead to large uncertainties in percentiles.

Furthermore, $\mathrm{WDR3_3}$-based exposure maps for Canada are developed based on four risk categories as follows: Sheltered ($\mathrm{WDR3_3} \leq 33\ \mathrm{L/m^2}$); Moderate ($33 \leq \mathrm{WDR3_3} \leq 56.5\ \mathrm{L/m^2}$); Severe ($56.5 \leq \mathrm{WDR3_3} \leq 100\ \mathrm{L/m^2}$); Very severe ($\mathrm{WDR3_3} \geq 100\ \mathrm{L/m^2}$). The thresholds used to identify risk categories are based on BRE Report BR262 (BRE, 2002); since water penetration also depends on several other variables such as the type of façade material and insulation, appropriate adjustments to thresholds may be required.

3.3.2 Validation and projected changes

For validating the wind field, the mean annual wind speeds and their inter-annual variability based on GEM-ERA-Interim simulation are compared with those from ERA5 and ERA-Interim reanalysis for the 1981–2010 period. As for rain, the annual, fall and summer mean rainfall based on the same simulation are compared to the validation datasets. However, as rainfall is not available for ERA-Interim and CRU, comparison is performed only for summer.

Moreover, GEM-ERA-Interim is also compared with GEM-CanESM2 to evaluate boundary forcing errors, i.e. to assess the impact of errors in the driving CanESM2 data. Since larger portions of the WDR loads occur in Fall and summer, analysis to follow will focus on these seasons.

As wind direction plays an important role in determining wind-driven rain, it is also validated for the sixteen locations considered in this study by comparing GEM-ERAInterim-simulated wind directional distribution with point observations (wind roses) at these locations. These comparisons are undertaken considering all hourly values as well as for rainy hours. ERA5 derived wind directional distributions are also used in validation.

Projected changes to WDR-related variables and WDR characteristics are obtained by comparing GEM_CanESM2 ensemble averaged values of for the future 1981-2010 period with those for the current 2071-2100 period. The ensemble averages provide better estimates compared to any of the individual simulations and model spread is used where appropriate to quantify uncertainties.

3.4 Validation

3.4.1 Validation of Model Simulated Fields

Prior to the investigation of projected changes to WDR characteristics, the ability of the model in simulating rain and wind characteristics is investigated. Fig. 3.2 shows the spatial patterns of mean annual, summer (JJA) and fall (SON) rainfall obtained from ERA-Interim and ERA5 reanalysis datasets, and two GEM simulations, for the 1981-2010 period. ERA5 shows high values of mean annual rainfall along the west coast and south eastern regions, and lower values for the northern regions, as expected. ERA-Interim generally shows higher values of mean summer rainfall than ERA5 and CRU, particularly for the eastern parts of Canada. The GEM-ERAInterim simulation captures the spatial patterns of mean annual and seasonal rainfall reasonably well and agrees better with ERA5 compared to ERA-Interim for summer, suggesting added value in downscaling ERA-Interim reanalysis. The GEM-CanESM2 also captures well the rainfall spatial patterns, albeit the underestimation of summer rainfall for the southern Canadian regions. This can be partly attributed to the biases in the driving CanESM2 data, particularly in the humidity field, and the closeness of this region to the southern boundary of the experimental domain.

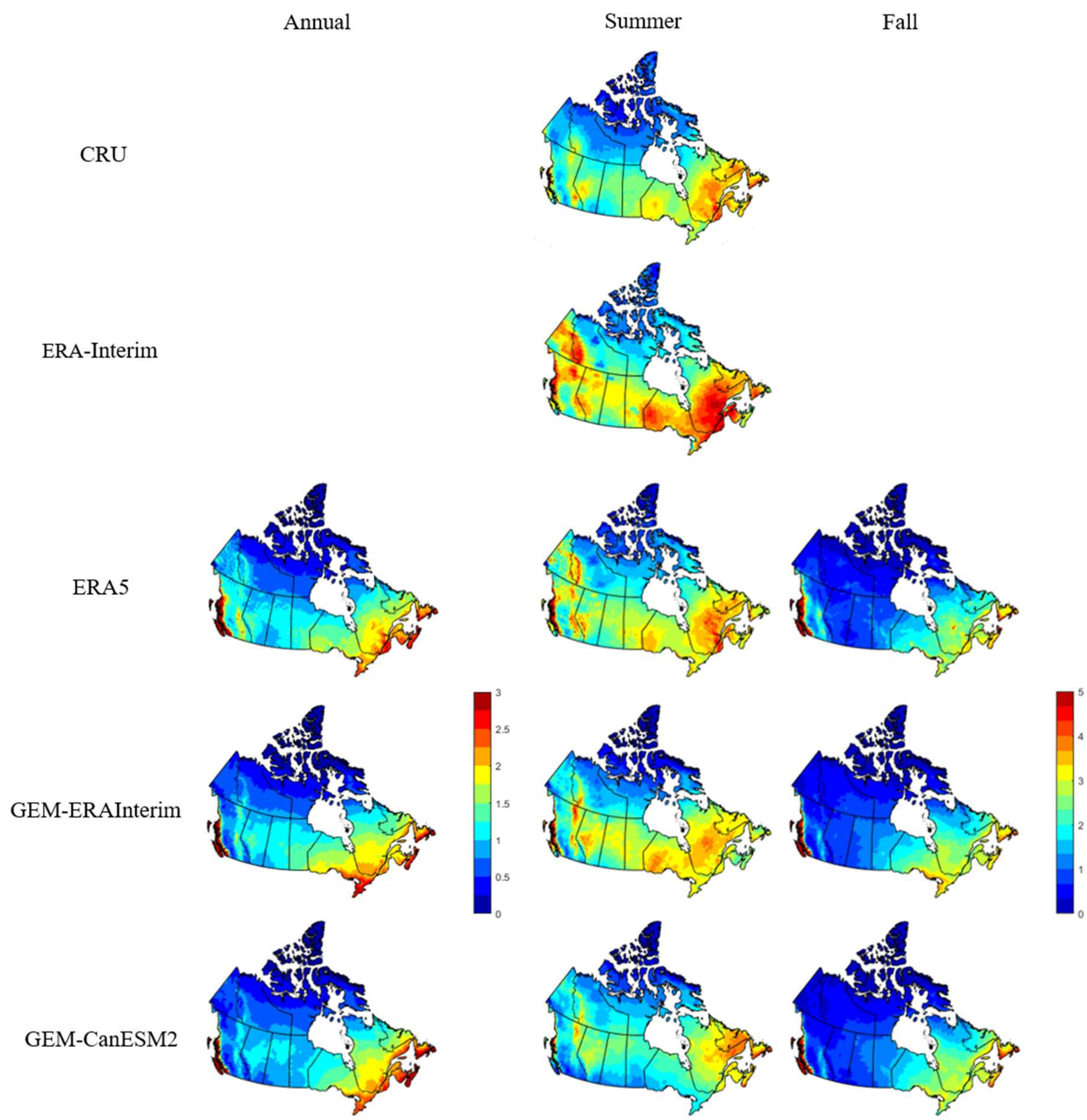

Figure 3.2 Annual, summer (JJA) and fall (SON) mean rainfall (mm/day) for ERA5 and two GEM simulations for the 1981-2010 period. Also shown are the summer rainfall from CRU and ERA-Interim for the same period.

As for wind (Fig. 3.3), both ERA-Interim and ERA5 reanalysis show high annual, summer and fall mean wind speeds for the north central and eastern parts of Canada, whereas ERA5 displays reduced wind speed values over the western region of Canada compared to ERA-Interim, which is closer to observations as shown in Jeong and Sushama (2018). This is due to the higher resolution of ERA5, which enables better representation of topography and therefore roughness length, which is important for wind. Previous study by Zhao and Sushama (2020), using the same set of simulations as in this study, also came to the same conclusions. Although, the GEM-ERAInterim captures the spatial patterns of the annual and seasonal mean wind speed reasonably well, it shows generally lower mean wind speed values. GEM-ERAInterim wind magnitudes for the western mountainous region has however improved with downscaling. The GEM-CanESM2 simulation shows quite similar mean wind speed patterns to those of GEM-ERAInterim indicating that the boundary forcing errors are modest.

The directional distribution of wind speeds for sixteen urban centers are presented in Fig. 3.4. ERA5 exhibits high degree of agreement with point observations, except for Inuvik. It also shows slights differences for Vancouver where the observation station is located on the coastline. The wind directions for GEM-ERAInterim agree with ERA5 and observations. As the predominant wind direction may be quite different than prevailing wind direction during rain events (Surry et al., 1995), comparison of wind directions during rain events are also performed for the same locations (Fig. 3.5). The prevailing wind direction during rain events seems to be distinct than the predominant wind direction, especially for Toronto and Edmonton. The directional distribution of wind speed during rainy-hours is also distinct than that of all-hours for Charlottetown, Halifax and Inuvik. Again, the distribution of wind directions during rain events are captured well by the GEM simulation. Also, GEM-CanESM2 captures well the directional distribution of both rainy and all hours and show quite similar patterns to those of GEM-ERAInterim. However, it is important to note that the wind roses obtained from the two

GEM simulations are developed based on 3-hourly data compared to hourly data for point observations and ERA5 reanalysis, and therefore, wind magnitudes are smaller than those of ERA5 and observations, partly due to differences in the temporal resolution of the wind data. The relatively coarse spatial resolution of the model also contributes to the differences in the wind magnitudes and directions as it limits the ability of the model to capture the surface heterogeneity and therefore the surface wind patterns.

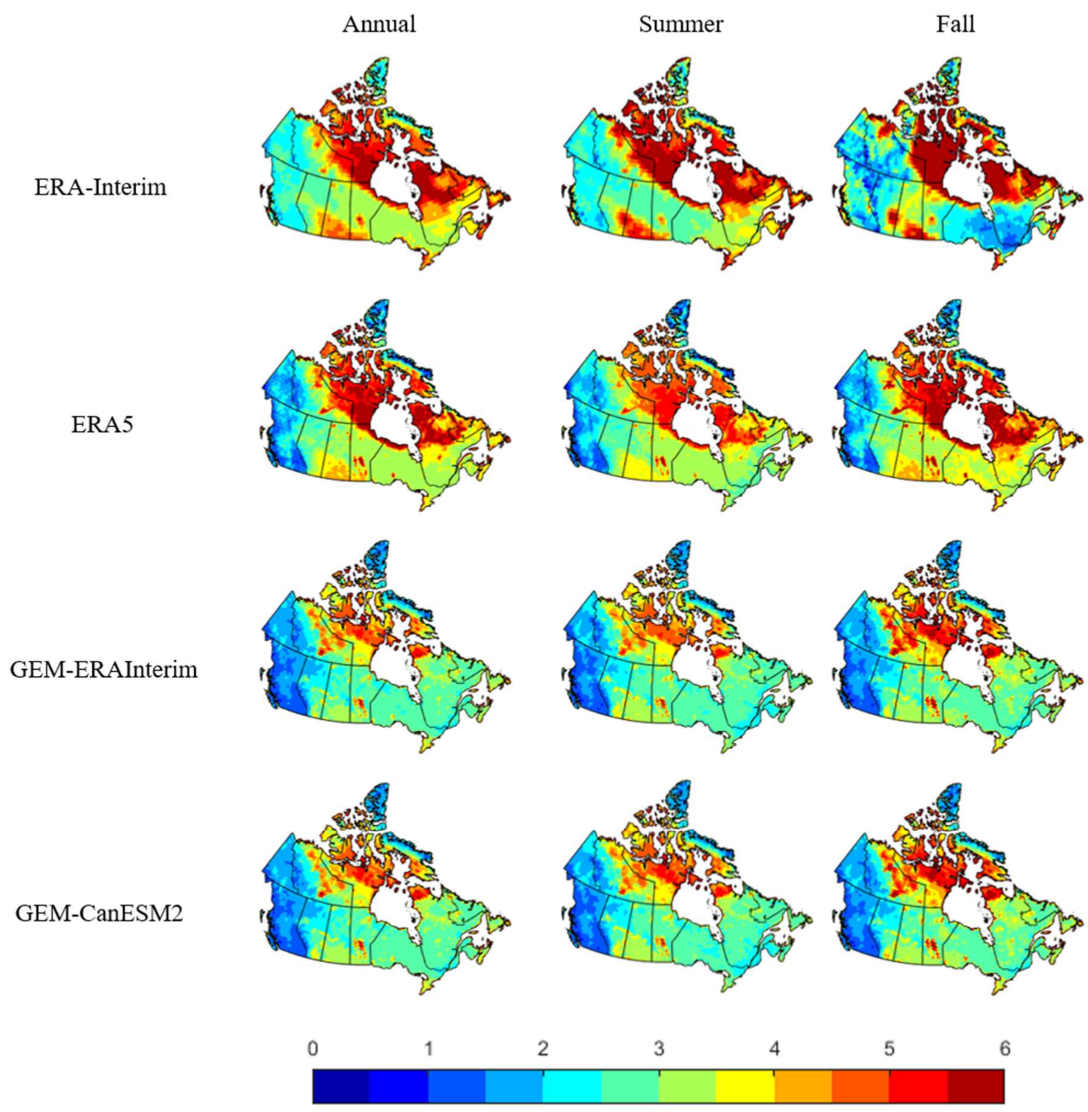

Figure 3.3 Annual, summer (JJA) and fall (SON) mean wind speed (m/s) for ERA-Interim reanalysis, ERA5, and two GEM simulations for the 1981-2010 period.

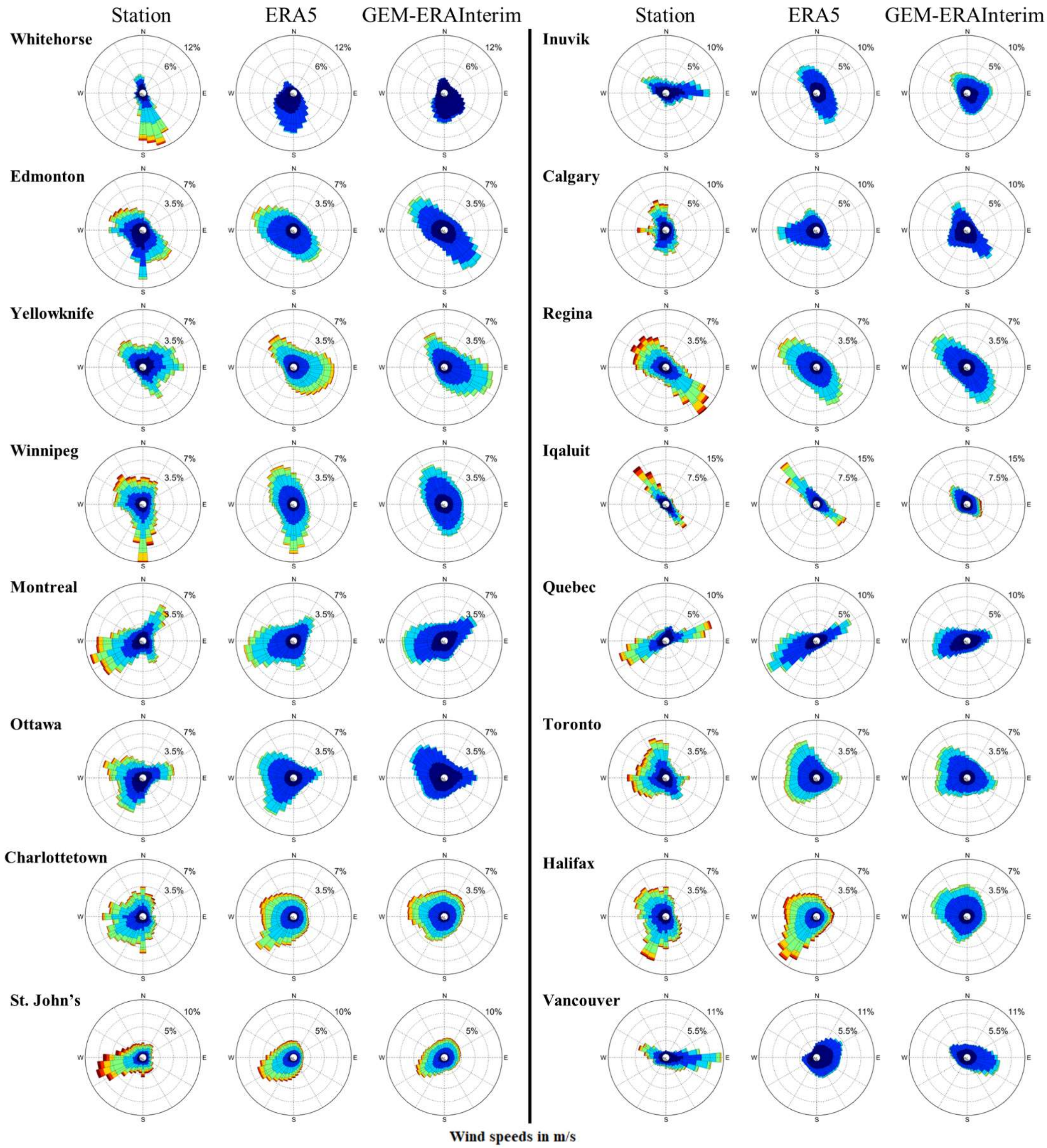

Figure 3.4 Directional distributions of wind speeds (m/s) for all hours for 16 Canadian cities derived from GEM-ERAInterim simulation, station observations and ERA5 reanalysis for the 1981-2010 period.

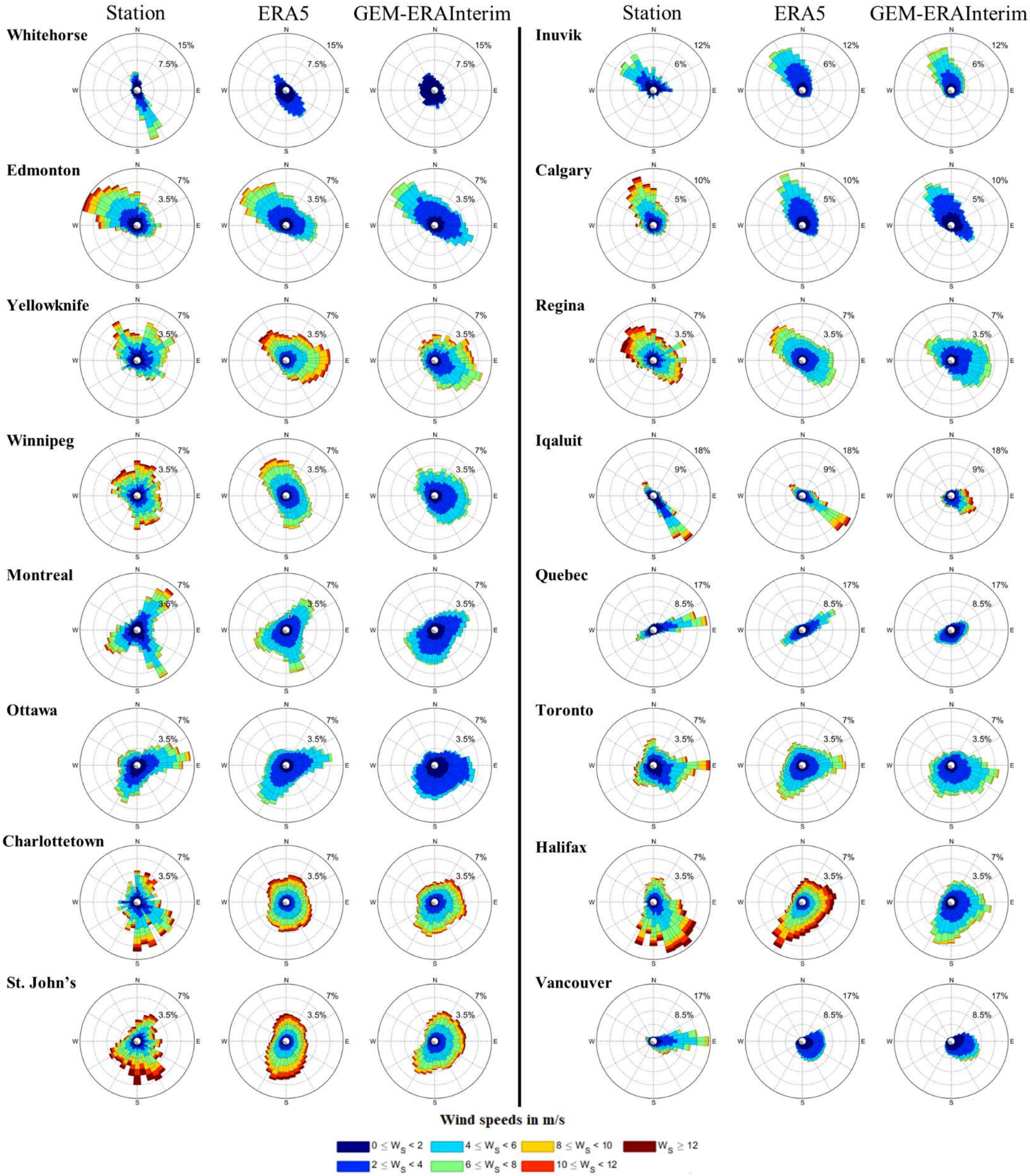

Figure 3.5 Directional distributions of wind speeds (m/s) for rainy hours for 16 Canadian cities derived from GEM-ERAInterim simulation, station observations and ERA5 reanalysis for the 1981-2010 period.

3.4.2 Validation of WDR loads

Analysis of the annual, summer and fall WDR1 loads over Canada show similar patterns for ERA5 and GEM-ERAInterim (Fig. 3.6.a), with maximum annual WDR1 loads noted for the south-eastern regions and south-western coastline. This is consistent with the results given in (Straube and Schumacher, 2006), who reported highest WDR for the eastern cities such as St. John, Sydney, Charlottetown, and Halifax as well as Vancouver on the west coast. Although GEM-ERAInterim shows high consistency with ERA5, it yields lower WDR1 values generally due to lower wind speeds in the model as discussed earlier, especially for the eastern region. The spatial patterns of WDR1 loads for the simulation driven by CanESM2 show similarities with those of GEM-ERAInterim overall, except for southern parts of Canada due to the underestimation of rainfall, particularly during summer. Furthermore, analysis of monthly WDR1 loads in ERA5 suggests that the maximum loads occur during the summer months for most regions of Canada, except for the western coastline which is exposed to more loads during the fall/early winter season, which coincides with the timing of maximum rainfall for this region (Fig. 3.6.b). GEM-ERAInterim and GEM-CanESM2 simulated timing match with those of ERA5. Overall, the GEM model is able to simulate the WDR1 loads and related climatic variables reasonably well, suggesting that it can be applied to study changing characteristics of these variables in transient climate change simulations. The model also captures reasonably well WDR spell characteristics, particularly frequency, spell duration, and intensity compared to those derived from ERA5. The above validation results provide confidence in using the model to assess projected changes to WDR characteristics.

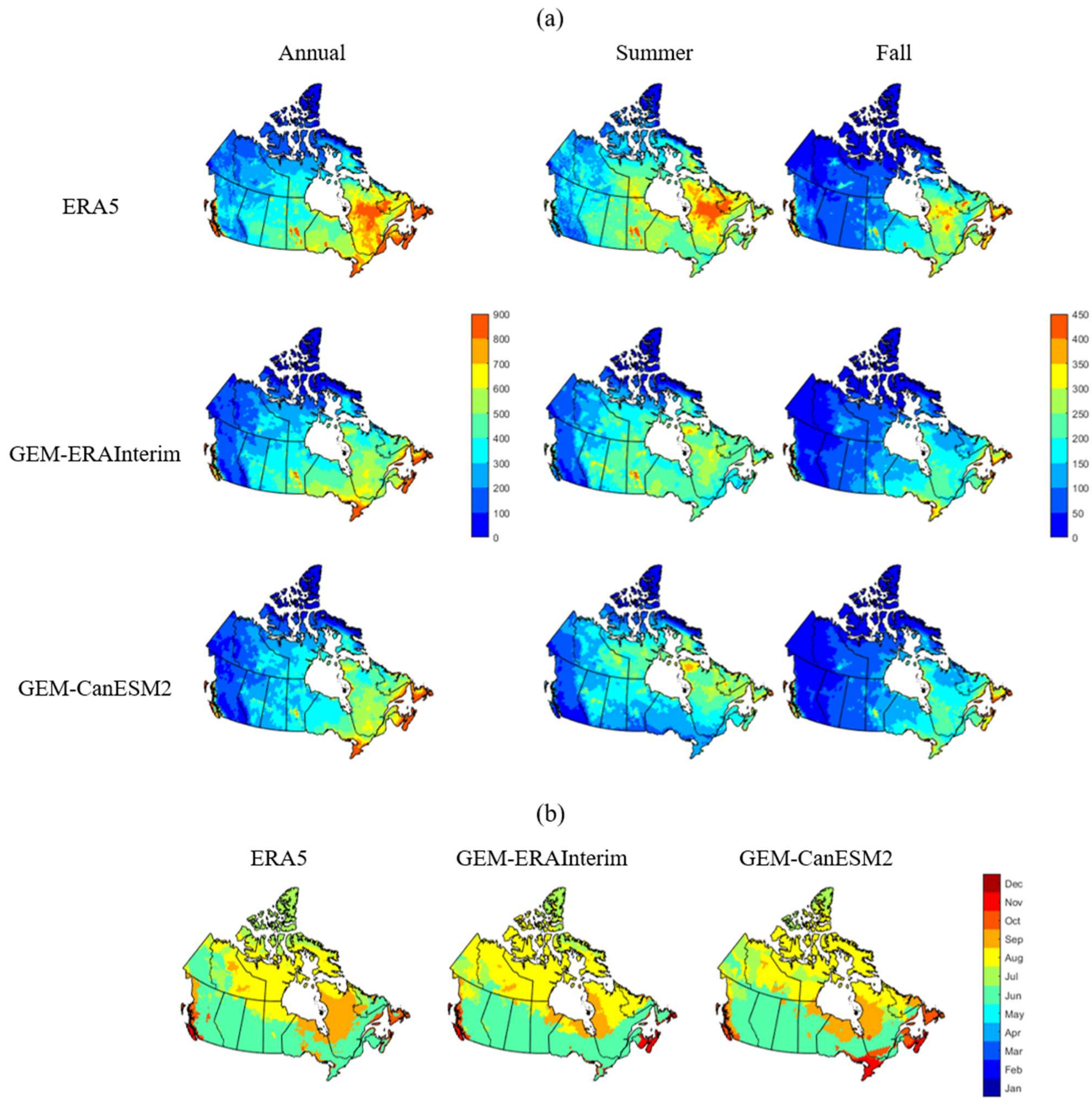

Figure 3.6 (a) Mean of total omnidirectional annual, summer (JJA) and fall (SON) WDR loads (mm/m2); (b) timing of maximum monthly WDR loads of ERA5, and two GEM simulations for 1981-2010 period.

3.5 Projected changes

3.5.1 WDR related climate variables

Analysis of projected changes to annual, summer and fall rainfall are presented in Fig. 3.7. Relatively larger increases are found in fall for the eastern regions and along the western coast. Also, the rainfall during winter is expected to significantly increase for the south-eastern parts of Canada (figure not shown). However, the south-central regions and the western coastline will experience reduced summer rainfall in the future. Annually, increases are therefore noted, except for the south central regions. As for wind, the mid-northern parts of Canada will experience higher mean wind speed during rain events in summer and fall in the future, but noteworthy decreases are noted for the southern and eastern regions of Canada (Fig. 3.8). More-or-less similar pattern can be observed for the mean annual wind speed, with projected changes near zero for the southern regions, which is linked to increased rain to snow ratio during winter and spring and associated increases in wind magnitudes in future for these periods during rain events. No significant changes to the directional distribution of wind speed during rain events are projected (figure not shown). Overall, changes in wind speeds are expected to have moderate impacts on future WDR loads.

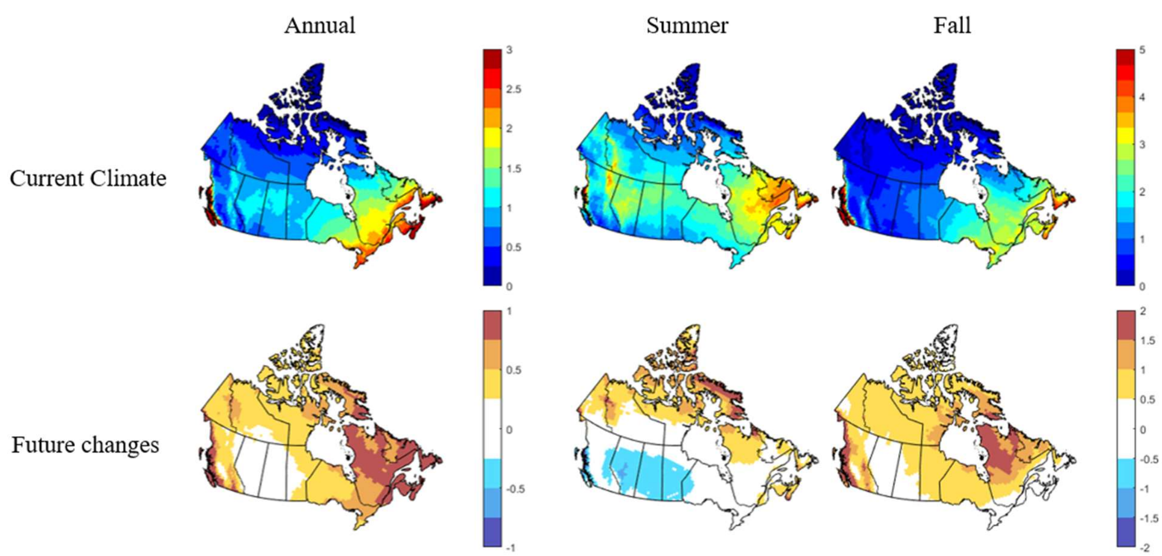

Figure 3.7 Projected changes to the annual, summer (JJA) and fall (SON) mean rainfall (mm/day) obtained for GEM-CanESM2 simulation, for the future 2071-2100 period with respect to the current 1981-2010 period.

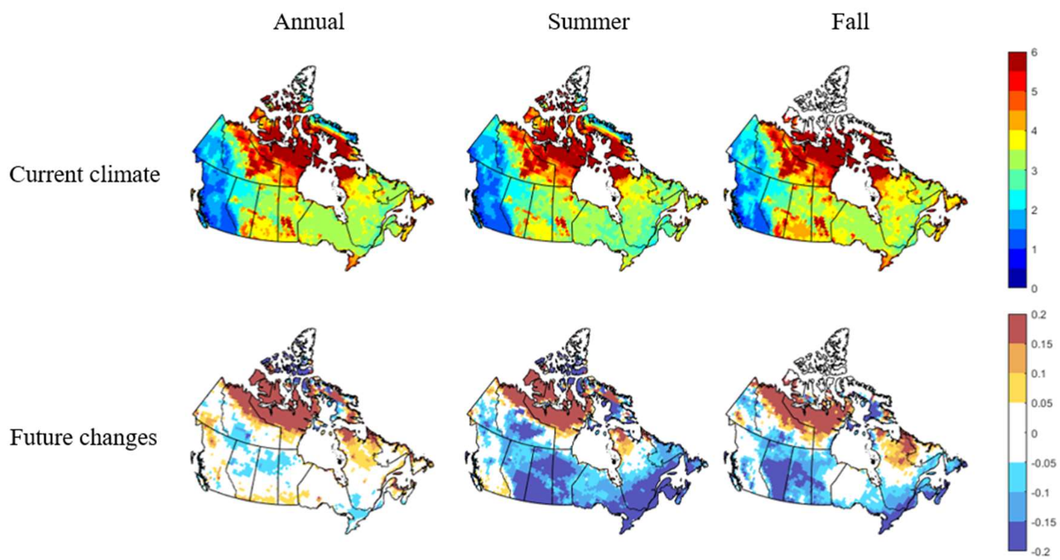

Figure 3.8 Projected changes to the annual, summer (JJA) and fall (SON) mean wind speed (m/s) during rain-events only obtained for GEM-CanESM2 simulation, for the future 2071-2100 period with respect to the current 1981-2010 period.

3.5.2 WDR1 loads

Mean annual, summer and fall WDR1 loads and the projected changes to these loads are presented in Fig. 3.9(a). Based on the results of GEM-CanESM2 simulation, increases in future WDR1 loads are projected for eastern, northern and western coastline regions of Canada for fall. Most regions will experience no changes or reduced loads during summer (i.e. the most critical season in current climate). The annual changes for future therefore suggest an overall increase mostly. The projected decreases in summer hints at potential changes in the timing of maximum monthly loads, which is confirmed by the timing patterns presented in Fig. 3.9(b) for current and future climates. Many regions will be exposed to higher loads later during the year than in current climate. For instance, the regions south of the Hudson's Bay will see a shift in the timing from late summer and early fall to late fall. Though temperatures will be warmer in future than in current climate, evaporation rates are still lower during the latter part of the fall compared to the earlier part. This is suggestive of increased moisture content of facades. This shift in timing of maximum WDR1 loads to cooler months will therefore be more critical for building envelope. However, the duration of the WDR events is also important and will be discussed below in Section 3.5.4.

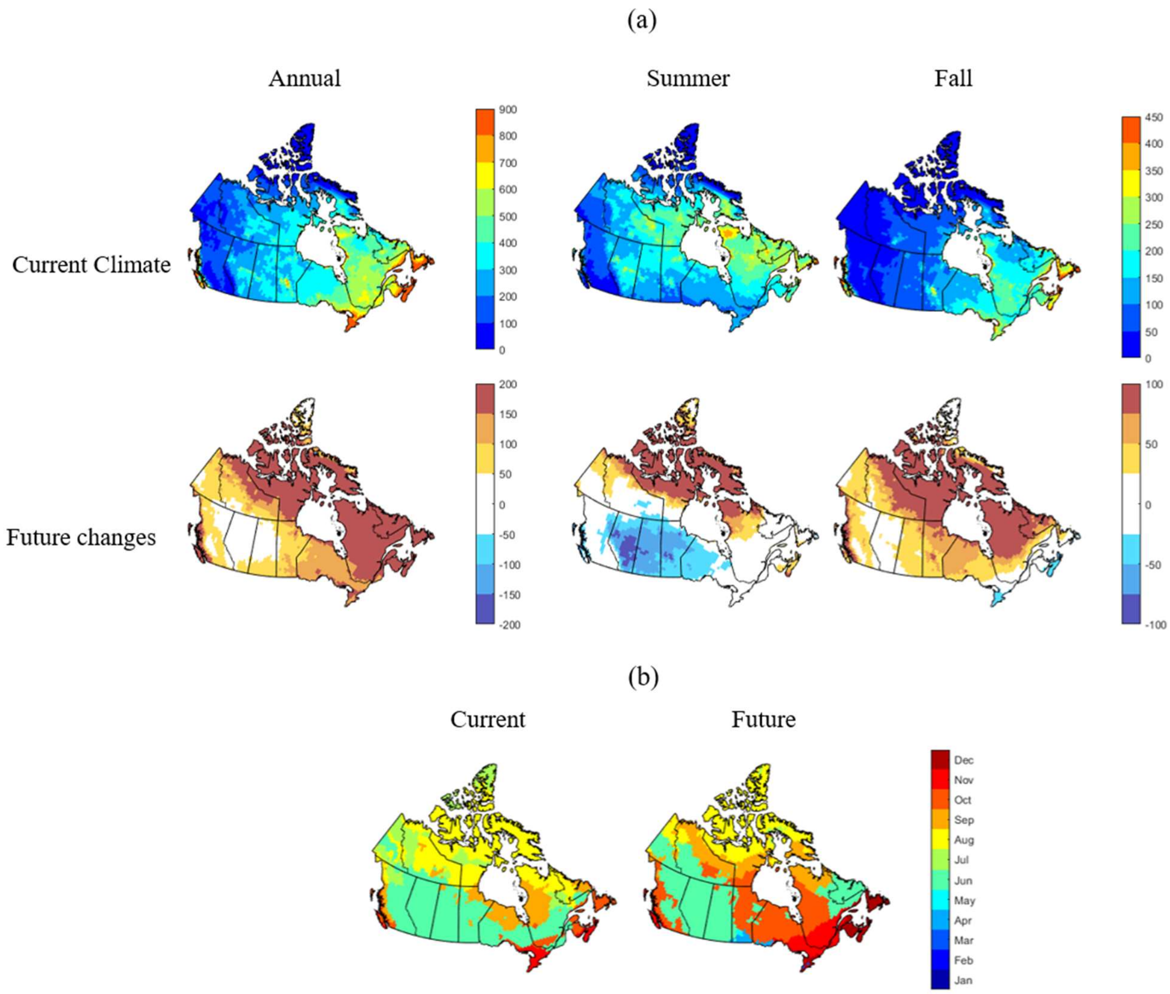

Figure 3.9 (a) Projected changes to total annual, summer (JJA) and fall (SON) WDR loads (mm) obtained from GEM-CanESM2 simulation, for the future 2071-2100 period with respect to the current 1981-2010 period. (b) Current and future timing of maximum monthly WDR loads.

3.5.3 WDR2 loads

The mean annual WDR2 loads deposited on a building facade at 10 m above grade in an open terrain for eight façade orientations (N, NE, E, SE, S, SW, W, NW) and their projected changes based on CanESM2 simulations are investigated in Fig. 3.10. By the end of the century, eastern and northern parts of Canada will be exposed to higher WDR2 loads, irrespective of the façade orientation. North and north-west oriented façades will be subject to smaller increases in WDR2 loads, generally, compared to other orientations. For west-coast regions, larger increases in WDR2 loads will be for facades facing south to east. Central regions generally show no changes to WDR2 loads. However, it is important to note that the amount of WDR2 of a specific building in a given region can be greater or less than the shown values due to building geometry and surrounding buildings.

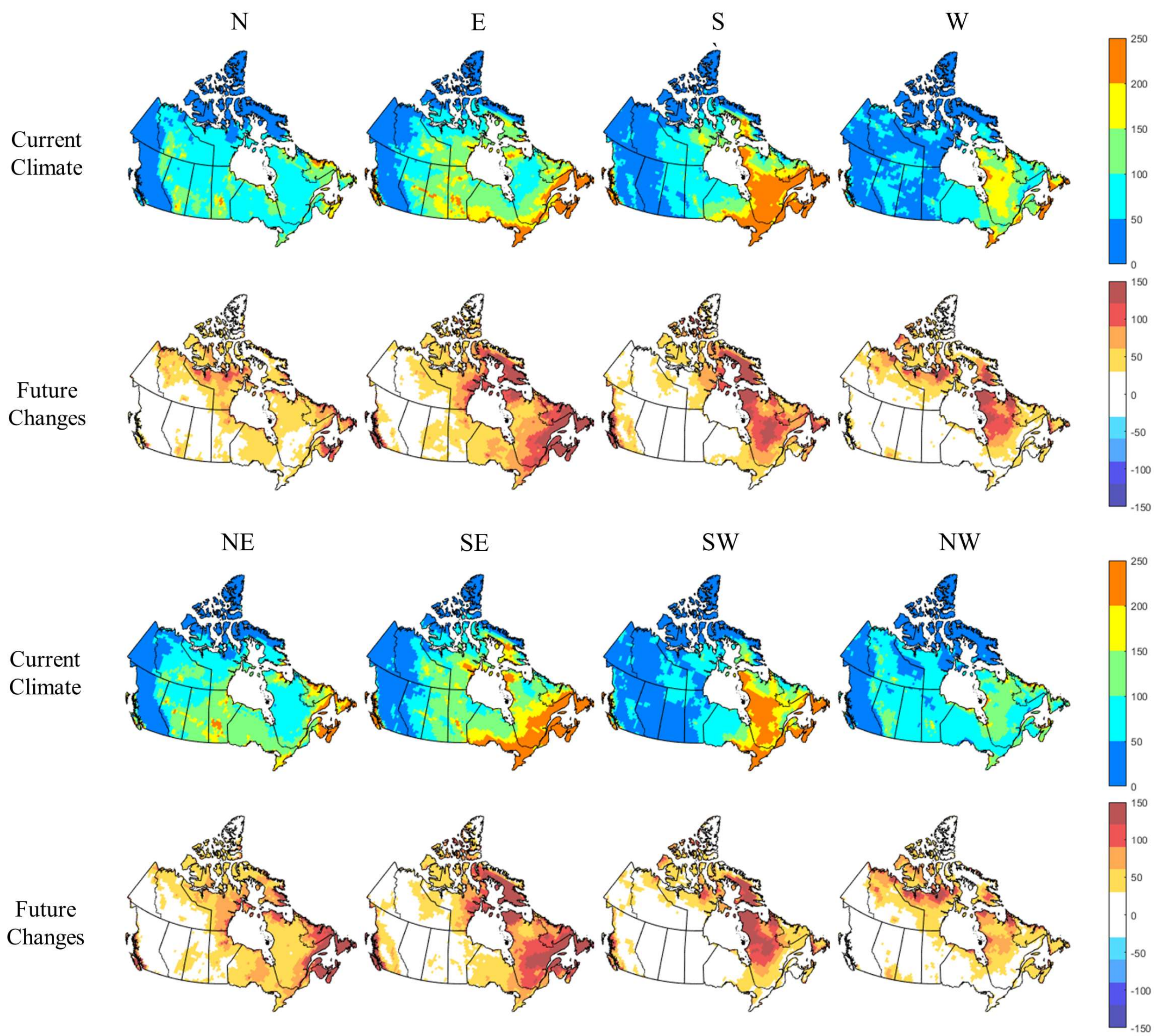

Figure 3.10 The amount of WDR loads deposited on a generic building façade (L m-2) for 16 orientations and the projected changes to these loads based on GEM-CanESM2 simulation for the future 2071-2100 period with respect to the current 1981-2010 period.

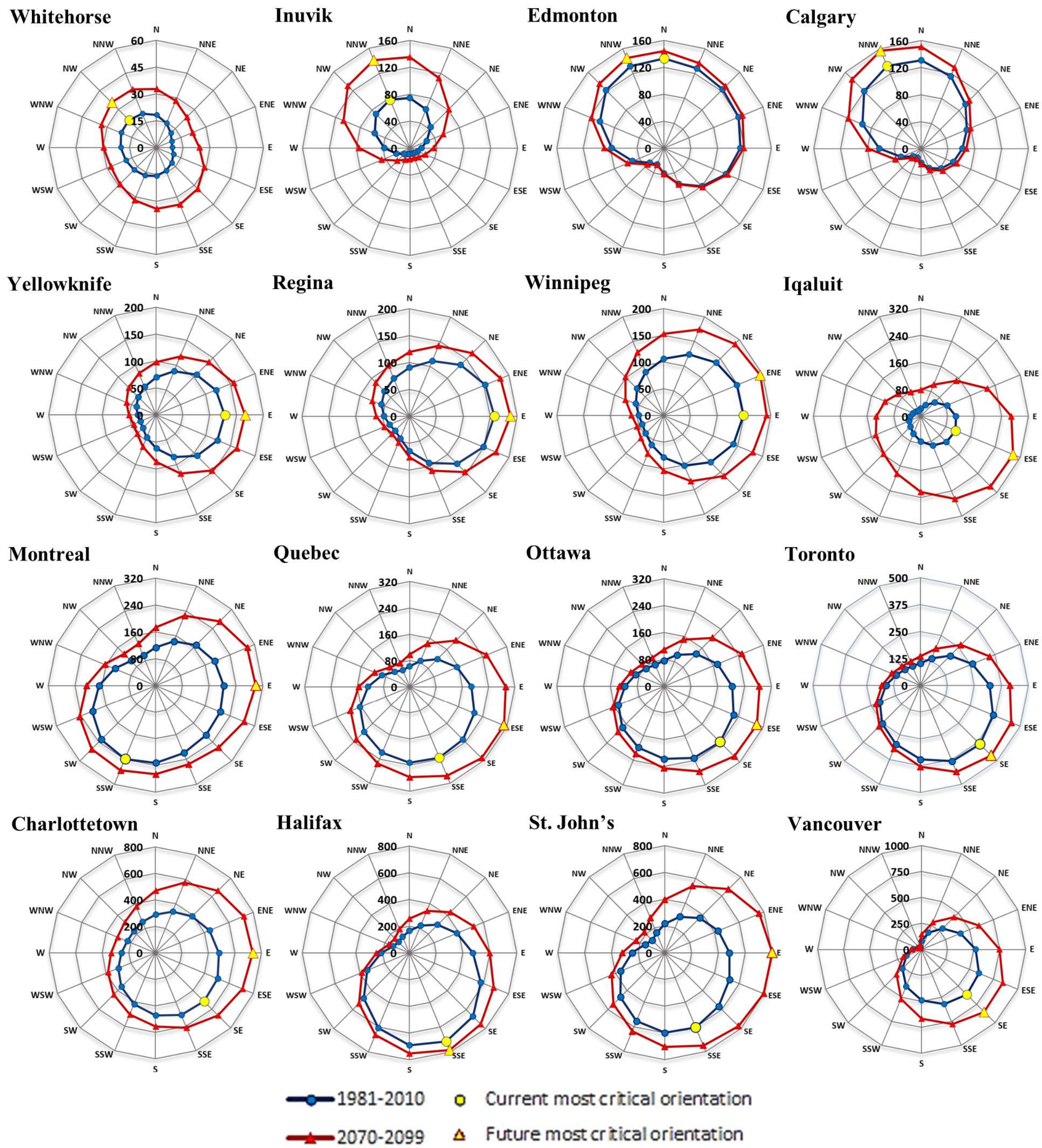

Figure 3.11 Annual WDR loads deposited on differently oriented building facades (L m-2) at 10m above grade in an open terrain for 16 Canadian cities for the 1981-2010 (blue) and 2071-2100 (red) periods and the worst façade orientation indicated for current and future climates.

Detailed results for WDR2 loads, for current and future climates, for the sixteen Canadian cities/locations considered in this study, are presented in Fig. 3.11. The future WDR2 loads exhibit changes to the critical façade direction for some cities in future climate, with Montreal showing the biggest directional change. The current critical direction for building facades in Montreal is south-south-west, while, in future, the critical direction will be east, with a 48% increase in load for this direction. Other locations with projected changes in critical façade orientations are Edmonton, Winnipeg, Quebec, Ottawa, Charlottetown and St. Johns. Generally, all cities will experience increases in WDR2 loads, for most of the directions. The largest absolute WDR2 loads in current and future climates are for Vancouver and the maritime cities Halifax and St. John's. The least WDR2 loads in current and future climates will be for Whitehorse. The projected changes to WDR2 loads are the least for Edmonton. In the north, although larger relative increases in WDR loads are noted for Yellowknife and Inuvik, these cities are still among the least exposed cities to WDR2. However, significant increases to WDR2 loads are suggested for Iqaluit leading to more severe exposure levels. It is important to mention here that the directional distribution will vary within the city, from one location to another, due to local turbulence and wind deformation induced by surrounding buildings.

3.5.4 WDR3 loads and exposure category maps

The scatterplots of WDR3 and spells durations for future critical facades for the sixteen locations for current and future periods, and their respective distribution functions, are presented in Fig. 3.12. Most cities will experience longer WDR spells and larger WDR3 loads in future climate. The scatterplots also illustrate more extreme WDR spell events (i.e. high WDR3 loads in short durations). Table 1 quantifies projected changes to selected statistics (i.e. median and 95th percentile) of WDR3 duration, magnitude and intensity, which suggests generally increases except for some south central cities. Analysis of WDR3 extreme spell events, i.e. spells greater than 95th percentile values of duration, magnitude and intensity, also shown in Table 1, suggest increases in duration and magnitude, but decreases in intensity for nine out of the sixteen locations. The increase in the intensity and/or amount of WDR spell loads lead to higher probability of rain penetration and damage risks. Consequently, more restrictive standards regarding the requirements of building envelope construction, finishing, and materials and insulation used should be applied.

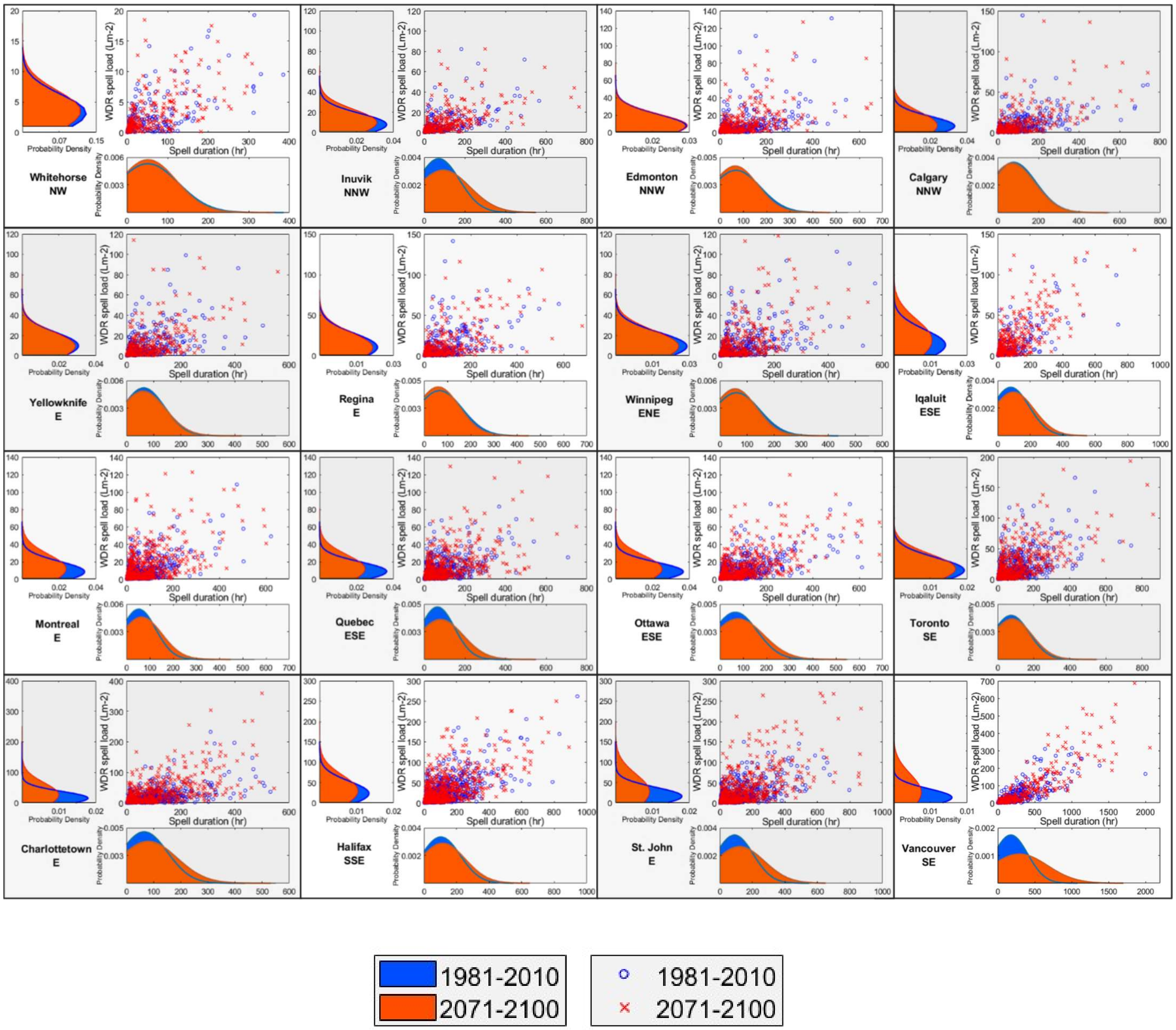

Figure 3.12 Amount and duration of WDR3 loads for the future most critical façade orientation along with probability density functions for WDR3 amount and duration for 16 selected cities for the 1981-2010 (blue) and 2071-2100 (red) periods.

City (Critical orientation)	Duration (hr)		Amount (L m^{-2})		Intensity (mm/s)		WDR extreme spell events		
	Median	95th Percentile	Median	95th Percentile	Median	95th Percentile	Mean duration	Mean amount	Mean intensity
Montreal (E)	19	189	2.85	30.78	0.11	0.93	189	47.18	0.55
	37%	28%	34%	41%	23%	9%	17%	41%	12%
Vancouver (SE)	93	650	10.06	129.53	0.12	0.42	803	209.68	0.30
	34%	77%	31%	140%	7%	7%	57%	101%	19%
Toronto (SE)	31	271	5.05	52.88	0.15	1.06	274	82.11	0.67
	19%	3%	28%	23%	4%	20%	3%	12%	-10%
Edmonton (NNW)	24	282	1.79	26.37	0.09	0.67	268	53.74	0.40
	-6%	-12%	1%	17%	6%	-14%	-18%	-1%	-3%
Calgary (NNW)	28	296	2.24	29.73	0.09	0.60	280	45.60	0.41
	-33%	-4%	-17%	16%	3%	-1%	11%	42%	1%
Ottawa (ESE)	23	247	3.26	28.18	0.10	0.71	264	42.79	0.24
	39%	21%	23%	61%	2%	13%	22%	51%	47%
Regina (E)	29	248	2.66	41.31	0.12	0.83	267	67.46	0.58
	-38%	-3%	-23%	10%	3%	-8%	-10%	9%	-21%
Quebec (ESE)	29	227	3.54	29.62	0.10	0.79	193	43.13	0.51
	21%	33%	39%	43%	6%	5%	52%	49%	-24%
Winnipeg (ENE)	24	238	2.56	36.01	0.11	0.77	179	55.24	0.56
	-21%	-10%	-19%	17%	5%	-4%	16%	15%	-18%
Halifax (SSE)	65	323	10.72	76.02	0.19	1.29	315	117.87	0.56
	5%	30%	25%	37%	7%	14%	24%	28%	15%
Charlottetown (E)	25	228	6.28	54.71	0.18	1.50	228	87.82	0.53
	36%	30%	47%	86%	31%	20%	31%	84%	46%
St john’s (E)	48	332	6.37	64.62	0.14	1.48	312	88.70	0.40
	50%	22%	50%	62%	0%	-14%	29%	97%	98%
Whitehorse (NW)	31	271	5.05	52.88	0.15	1.06	274	82.11	0.67
	19%	3%	28%	23%	4%	20%	3%	12%	-10%
Yellowknife (E)	32	213	4.07	34.21	0.12	0.81	177	52.50	0.51
	-22%	1%	-21%	3%	4%	-19%	38%	5%	-10%
Inuvik (NNW)	25	290	2.61	25.52	0.10	0.51	270	44.93	0.36
	92%	8%	37%	32%	-14%	1%	27%	14%	-9%
Iqaluit (ESE)	28	297	4.91	49.00	0.13	0.96	325	73.37	0.65
	68%	16%	54%	49%	30%	8%	21%	38%	-44%

Table 1: Characteristics (Duration, amount and intensity) of WDR3 loads and extreme spell events of the future most critical orientation for 16 Canadian cities and their projected changes for the 2071-2100 period with respect to the current 1981-2010 period.

Fig. 3.13 shows the WDR3$_3$-based risk category maps for different façade orientations for the current and future periods. Current risk category maps indicate that most regions of Canada fall within the sheltered and moderate categories, particularly for north and west oriented facades. As illustrated, projected changes to WDR3$_3$ loads are significant such that it transforms many regions to more severe risk categories (i.e. severe and very severe categories), particularly for south and east oriented building facades in the eastern parts of Canada. $WDR3_3$ loads and risk categories for current and future climates for the 16 cities considered in this study are summarized in Table 2. Although some cities fall under the very severe risk category currently for specific façade orientation, the large increase in future $WDR3_3$ loads are crucial and should be considered, especially for east oriented facades in Vancouver which will experience three times higher values.

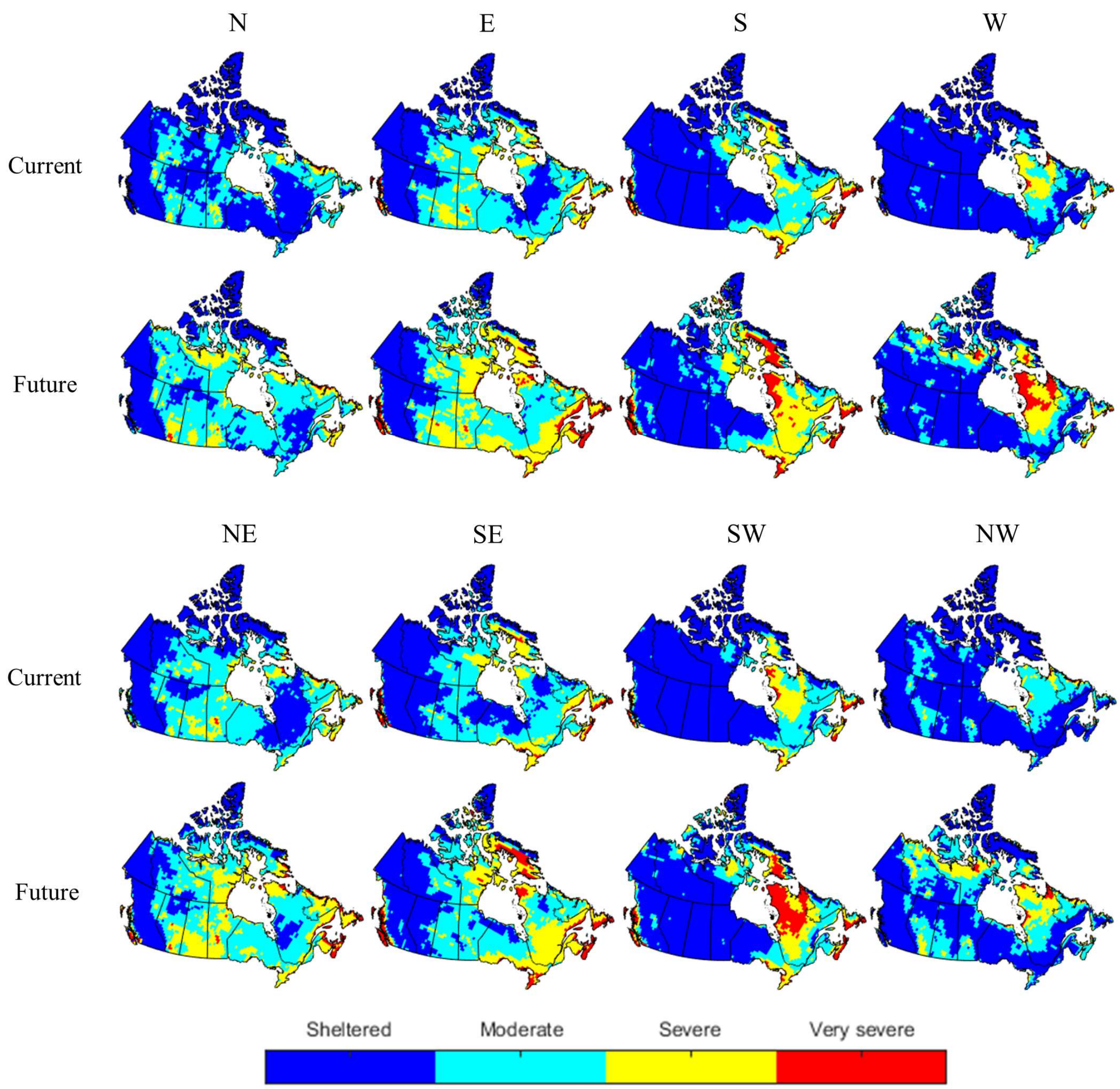

Figure 3.13 WDR exposure zones in Canada for different building facades orientations for the 1981-2010 and 2071-2100 periods.

City	N Spell	N Zone	E Spell	E Zone	S Spell	S Zone	W Spell	W Zone
Montreal	34	R2	49	R2	45	R2	34	R2
	47	**R2**	**73**	**R3**	**49**	**R2**	**37**	**R2**
Vancouver	22	R1	146	R4	187	R4	28	R1
	43	**R2**	**291**	**R4**	**302**	**R4**	**35**	**R2**
Toronto	36	R2	90	R3	79	R3	37	R2
	40	**R2**	**102**	**R4**	**83**	**R3**	**40**	**R2**
Edmonton	48	R2	47	R2	15	R1	32	R1
	55	**R2**	**47**	**R2**	**13**	**R1**	**33**	**R1**
Calgary	48	R2	35	R2	9	R1	22	R1
	67	**R3**	**44**	**R2**	**8**	**R1**	**33**	**R1**
Ottawa	23	R1	49	R2	42	R2	22	R1
	30	**R1**	**68**	**R3**	**51**	**R2**	**24**	**R1**
Regina	41	R2	64	R3	19	R1	14	R1
	60	**R3**	**76**	**R3**	**21**	**R1**	**25**	**R1**
Quebec	22	R1	47	R2	47	R2	23	R1
	25	**R1**	**70**	**R3**	**57**	**R3**	**28**	**R1**
Winnipeg	49	R2	47	R2	23	R1	16	R1
	58	**R3**	**57**	**R3**	**31**	**R1**	**23**	**R1**
Halifax	44	R2	95	R3	135	R4	41	R2
	74	**R3**	**143**	**R4**	**159**	**R4**	**61**	**R3**
Charlottetown	74	R3	106	R4	82	R3	51	R2
	116	**R4**	**177**	**R4**	**86**	**R3**	**57**	**R3**
St john’s	69	R3	94	R3	129	R4	57	R3
	97	**R3**	**173**	**R4**	**149**	**R4**	**60**	**R3**
Whitehorse	8	R1	3	R1	6	R1	9	R1
	11	**R1**	**8**	**R1**	**10**	**R1**	**11**	**R1**
Yellowknife	30	R1	46	R2	18	R1	13	R1
	35	**R2**	**50**	**R2**	**26**	**R1**	**15**	**R1**
Inuvik	32	R1	8	R1	4	R1	18	R1
	41	**R2**	**16**	**R1**	**6**	**R1**	**25**	**R1**
Iqaluit	17	R1	57	R3	38	R2	24	R1
	42	**R2**	**88**	**R3**	**86**	**R3**	**65**	**R3**

Table 2: The volume of 3-year return level WDR spell (L m-2) deposited on building envelope and the WDR spell exposure zone for 16 Canadian cities for the main 4 façade orientations for the 1981-2010 (Light font) and 2071-2100 (**Bold font**) periods.

3.6 Summary and conclusion

In this study, the impact of climate change on wind and rain and the resulting changes in WDR loads across Canada are assessed for the future 2071–2100 period with respect to 1981–2010 period, using a five-member ensemble of GEM, driven by five different members of a CanESM2 ensemble corresponding to RCP8.5 scenario. Three different definitions of WDR loads are considered in this study: Omnidirectional WDR loads, directional WDR loads deposited on differently oriented facades and WDR spell loads. Comparison of rain, wind, and WDR loads obtained from an ERA-Interim driven GEM simulation to those obtained from ERA-Interim and ERA5 datasets for the current 1981–2010 period confirms the model's ability in reproducing these fields. This assessment also demonstrates added value in downscaling ERA-Interim reanalysis, which is particularly reflected in the distribution of rain events. The GEM-CanESM2 performs similarly to GEM-ERAInterim for wind speed and direction, while differences are noted for rain, especially for southern parts of Canada during summer.

Analysis of projected changes suggests large increases to WDR1 loads for the south-eastern and west coast regions, which is primarily due to changes in rainfall. Wind speed and direction changes are relatively less significant for most parts of Canada, except for the northern regions. Analysis also indicates that the timing of maximum monthly WDR1 loads shift from summer to fall in the future for the eastern regions of Canada. This will be more hazardous for building facades since evaporation rate is low during fall. The increase in winter WDR1 loads as well as the shift in the timing of these loads to late fall indicate potentially greater frost damage risk. Furthermore, WDR2 loads on differently oriented facades are also subjected to large increases in the future, particularly for the most critical façade orientations for coastal cities, while very smaller changes are noted for cities in the Canadian prairie region.

Furthermore, Results show large increases in spell duration and larger WDR3 loads for most cities. Also, more intense WDR3 events are suggested in future climate. $WDR3_3$ – based maps of risk categories suggest transformation of regions from low to high risk categories; this would imply more restrictions on the materials and insulation used for building facades. Therefore, specific guidance for designing for future $WDR3_3$ loads is needed along with recommendations for requirements and specifications. $WDR3_3$ values might be underestimated due to the underestimation of wind values, as discussed before, hence, many regions can be in higher risk categories.

To better understand the projected changes to WDR loads, higher resolution model simulations should be used to capture wind speed and direction more realistically. Furthermore, multi-GCM-RCM combinations based assessments for different emission scenarios should be undertaken to better quantify uncertainties.

Acknowledgements

This research was funded by the Natural Sciences and Engineering Research Council of Canada and the Trottier Institute for Sustainability in Engineering and Design. The simulations considered in this study were performed on the supercomputer managed by Calcul Québec and Compute Canada.

References

Bélair, S., Mailhot, J., Girard, C., and Vaillancourt, P. (2005). Boundary Layer and Shallow Cumulus Clouds in a Medium-Range Forecast of a Large-Scale Weather System. *Monthly Weather Review, 133*(7), 1938-1960. doi:10.1175/MWR2958.1

Benoit, R., Côté, J., and Mailhot, J. (1989). Inclusion of a TKE Boundary Layer Parameterization in the Canadian Regional Finite-Element Model. *Monthly Weather Review, 117*(8), 1726-1750. doi:10.1175/1520-0493(1989)117<1726:IOATBL>2.0.CO;2

Best, A. C. (1950). The Size Distribution of Raindrops. *Quarterly Journal of the Royal Meteorological Society, Vol. 76*, pp. 16-36.

Blocken, B., and Carmeliet, J. (2000). Driving Rain on Building Envelopes- I. Numerical Estimation and Full-Scale Experimental Verification. *Journal of Thermal Envelope and Building Science, 24*(1), 61-85. doi:10.1177/109719630002400104

Blocken, B., and Carmeliet, J. (2004). A review of wind-driven rain research in building science. *Journal of Wind Engineering and Industrial Aerodynamics, 92*, 1079-1130. doi:10.1016/j.jweia.2004.06.003

BRE. (2002). *Report BR262, Thermal insulation: avoiding risks*: IHS Press, Building Research Establishment.

Bush, E., and Lemmen, D. S. editors (2019): *Canada's Changing Climate Report*; Government of Canada, Ottawa, ON. 444 p.

Carbonez, K., Van Den Bossche, N., Ge, H., Lobelle, G., and Janssens, A. (2015). The Spell Definition in ISO-15927 and its Impact on the Rain Deposition on the Building Facade. *Energy Procedia, 78*, 2548-2553. doi:https://doi.org/10.1016/j.egypro.2015.11.274

Côté, J., Gravel, S., Méthot, A., Patoine, A., Roch, M., and Staniforth, A. (1998). The Operational CMC–MRB Global Environmental Multiscale (GEM) Model. Part I: Design Considerations and Formulation. *Monthly Weather Review, 126*(6), 1373-1395. doi:10.1175/1520-0493(1998)126<1373:TOCMGE>2.0.CO;2

Dee, D. P., Uppala, S., Adrian, S., Berrisford, P., Poli, P., Kobayashi, S., . . . Frédéric, V. (2011). *The ERA-Interim reanalysis: Configuration and performance of the data assimilation system – This report is superseded by the version published in Q J Roy Meteor Soc*. Retrieved from Shinfield Park, Reading: https://www.ecmwf.int/node/8946

Delage, Y. (1997). PARAMETERISING SUB-GRID SCALE VERTICAL TRANSPORT IN ATMOSPHERIC MODELS UNDER STATICALLY STABLE CONDITIONS. *Boundary-Layer Meteorology, 82*(1), 23-48. doi:10.1023/A:1000132524077

Dingle, N., and Lee, Y. (1972). Terminal Fallspeeds of Raindrops. *Journal of Applied Meteorology, 11*(5), 877-879. doi:10.1175/1520-0450(1972)011<0877:TFOR>2.0.CO;2

Diro, G., and Sushama, L. (2019). Simulating Canadian Arctic Climate at Convection-Permitting Resolution. *Atmosphere, 10*, 430. doi:10.3390/atmos10080430

Hans, H., Bell, W., Berrisford, P., Andras, H., Muñoz-Sabater, J., Nicolas, J., . . . Dick, D. (2019). Global reanalysis: goodbye ERA-Interim, hello ERA5. *ECMWF Newsletter*.

Harris, I., Osborn, T. J., Jones, P., and Lister, D. (2020). Version 4 of the CRU TS monthly high-resolution gridded multivariate climate dataset. *Scientific Data, 7*(1), 109. doi:10.1038/s41597-020-0453-3

Hersbach, H., and Dee, D. (2016). ERA5 reanalysis is in production. *ECMWF Newsletter, No. 147*, 7.

Hogberg, A. B., Kragh, M. K., and Van Mook, F. J. R. (1999). A comparison of driving rain measurements with different gauges. *Proceedings of the Fifth Symposium of Building Physics in the Nordic Countries*.

IPCC. (2013). *Climate Change 2013: The Physical Science Basis. Contribution of Working Group I to the Fifth Assessment Report of the Intergovernmental Panel on Climate Change* (T. F. Stocker, D. Qin, G.-K. Plattner, M. Tignor, S. K. Allen, J. Boschung, A. Nauels, Y. Xia, V. Bex, & P. M. Midgley Eds.). Cambridge, United Kingdom and New York, NY, USA: Cambridge University Press.

ISO. (2009). *ISO 15927-3: 2009: Hygrothermal Performance of Buildings - Calculation and Presentation of Climatic Data – Part 3: Calculation of a Driving Rain Index for Vertical Surfaces from Hourly Wind and Rain Data*: International Standards Organisation.

Jeong, D. I., and Sushama, L. (2018). Projected changes to extreme wind and snow environmental loads for buildings and infrastructure across Canada. *Sustainable Cities and Society, 36*, 225-236. doi:https://doi.org/10.1016/j.scs.2017.10.004

Jeong, D. I., and Sushama, L. (2019). Projected Changes to Mean and Extreme Surface Wind Speeds for North America Based on Regional Climate Model Simulations. *Atmosphere, 10*, 497. doi:10.3390/atmos10090497

Kain, J. S., and Fritsch, J. M. (1992). The role of the convective "trigger function" in numerical forecasts of mesoscale convective systems. *Meteorology and Atmospheric Physics, 49*(1), 93-106. doi:10.1007/BF01025402

Lacy, R. E. (1965). Driving rain maps and the onslaught of rain on buildings. *Proc. of CIB/RILEM Symposium on Moisture Problems in Buildings, Helsinki, 1965*.

Li, J., and Barker, H. W. (2005). A Radiation Algorithm with Correlated-k Distribution. Part I: Local Thermal Equilibrium. *Journal of the Atmospheric Sciences, 62*(2), 286-309. doi:10.1175/JAS-3396.1

Mironov, D., Golosov, S., Heise, E., Kourzeneva, E., Ritter, B., Sceider, N., and Terzhevik, A. (2005). *FLake - A lake model for environmental applications.* Paper presented at the 9th Workshop on Physical Processes in Natural Water, Lancaster Univ. U. K., 4-6 Sept.

Mironov, D., Kourzeneva, E., Ritter, B., Schneider, N., and Terzhevik, A. (2010). Implementation of the lake parameterisation scheme FLake into numerical weather prediction model COSMO. *Boreal Environ. Res., 15*, 218-230.

Nik, V., Mundt-Petersen, O., Sasic Kalagasidis, A., and Wilde, P. (2015). Future moisture loads for building facades in Sweden: Climate change and wind-driven rain. *Building and Environment, 93, Part 2*, 362-375. doi:10.1016/j.buildenv.2015.07.012

Nore, K., Blocken, B., Jelle, B., Vincent Thue, J., and Carmeliet, J. (2007). A dataset of wind-driven rain measurements on a low-rise test building in Norway. *Building and Environment, 42*, 2150-2165. doi:10.1016/j.buildenv.2006.04.003

Orr, S. A., and Viles, H. A. (2018). Characterisation of building exposure to wind-driven rain in the UK and evaluation of current standards. *Journal of Wind Engineering and Industrial Aerodynamics, 180*, 88-97. doi:10.1016/j.jweia.2018.07.013

Orr, S. A., Young, M., Stelfox, D., Curran, J., and Viles, H. (2018). Wind-driven rain and future risk to built heritage in the United Kingdom: Novel metrics for characterising rain spells. *Science of The Total Environment, 640-641*, 1098-1111. doi:https://doi.org/10.1016/j.scitotenv.2018.05.354

Pakkala, T. A., Lemberg, A.-M., Lahdensivu, J., and Pentti, M. (2016). Climate change effect on wind-driven rain on facades. *Nordic Concrete Research, Publication NO. 54*, 31-49.

Riahi, K., Rao, S., Krey, V., Cho, C., Chirkov, V., Fischer, G., . . . Rafaj, P. (2011). RCP 8.5—A scenario of comparatively high greenhouse gas emissions. *Climatic Change, 109*(1), 33. doi:10.1007/s10584-011-0149-y

Straube, J. (1998). *Moisture Control and Enclosure Wall Systems.* (Ph.D. Thesis), University of Waterloo, Waterloo, Canada.

Straube, J., and Burnett, E. (1997). *Rain Control and Screened Wall Systems Rain Control and Screened Wall Systems*.

Straube, J., and Burnett, E. (2000). *Simplified prediction of driving rain deposition*.

Straube, J., and Schumacher, C. J. (2006). Driving rain loads for Canadian building design, Report for CHMC by University of Waterloo, Ottawa.

Sundqvist, H., Berge, E., and Kristjánsson, J. E. (1989). Condensation and Cloud Parameterization Studies with a Mesoscale Numerical Weather Prediction Model. *Monthly Weather Review, 117*(8), 1641-1657. doi:10.1175/1520-0493(1989)117<1641:CACPSW>2.0.CO;2

Surry, D., Skerlj, P. F., and Mikitiuk, M. J. (1995). An Exploratory Study of the Climatic Relationships between Rain and Wind, Boundary Layer Wind Tunnel report BLT-2230-1994 for Canada Mortgage and Housing Corporation.

Verseghy, D. (2009). CLASS—the Canadian land surface scheme (version 3.4): technical documentation.

Viessmann, W., Knapp, J. W., Lewis, G. L., and Harbaugh, T. E. (1977). *Introduction to Hydrology* (Second Edition): Harper and Row.

Zadra, A., McTaggart-Cowan, R., and Roch, M. (2012). *Recent Changes to the Orographic Blocking.* Seminar presentation, RPN, Dorval, Canada, 30 March.

Zhao, Y., and Sushama, L. (2020). Aircraft Takeoff Performance in a Changing Climate for Canadian Airports. *Atmosphere, 11*(4). doi:10.3390/atmos11040418

CHAPTER 4 CONCLUSIONS AND RECOMMENDATIONS

4.1 Conclusions

This thesis investigates projected changes to WDR loads on building façades in a warmer future climate across Canada, which can have significant impacts on the durability and performance of building façades. Different load types (i.e. Omni-directional, directional WDR loads over a period of interest as well as WDR loads during a spell) are considered to ensure better understanding of the WDR characteristics. In this study, the results are based on rainfall and wind data obtained from a five-member ensemble of GEM simulations for the current 1981-2010 and future 2071-2100 periods for RCP8.5 emission scenario. Validation of the regional climate model simulated WDR-related fields confirmed the ability of the model in reproducing most of the fields reasonably well; some underestimation of wind speed magnitudes was noted for some locations. This gave confidence in applying the model to assess the changing characteristics of WDR loads in the future.

The findings of this research suggest large increases in WDR loads for many regions of Canada, particularly the south-eastern region and south-west coastline. Changes in rainfall are the main cause of the increases in WDR loads (Fig. A.3). However, for Arctic Canada, increases in WDR loads are due to increases in both rainfall and wind speed. Also, no significant changes are noted for wind directions for the 16 locations considered in this study (Fig. A.4 and Fig. A.5). Decreases in summer WDR loads are projected for some south central regions. A shift in the timing of WDR loads to cooler months is noted for many regions which indicates higher moisture content of the absorbent surfaces, given the relatively lower evaporation rates in these periods. Consequently, this is suggestive of increased likelihood of rain penetration. Additionally, the increase in winter WDR loads implies potentially greater freeze-thaw damage risk (Fig. A.6).

Detailed analysis undertaken for sixteen cities across Canada provide additional information. Study of the annual directional WDR loads on building façades for these cities indicate large increases for critical façade orientations. More specifically, coastal cities such as Vancouver, Charlottetown and St. John's will experience large increases of 200-400 L m^{-2} for the most critical façade orientation. For cities in Quebec and Ontario, increases of 25-45% are suggested. Furthermore, characteristics of WDR spells are subject to changes in a warmer climate. Increased spell durations and larger spell amounts are projected for most cities. Also, building façades will experience more extreme WDR spell events which are characterised by large spell amounts in relatively short durations. This leads to large increases in the 3-year return-levels of annual maximum WDR spell load which is used to develop WDR risk category maps. Based on the developed maps for current and future climates, many regions that are in the low to moderate exposure categories in current climate, will be changed to severe and very severe categories in future climate (Fig. A.7). Therefore, current practices for building envelope materials and insulation need to be revised to factor in these future changes.

Overall, the changing characteristics of WDR loads in the future highlight the need to develop specific guidelines for designing building envelopes along with recommendations for requirements and specifications. It also emphasizes the need to apply maintenance procedure for many existing buildings, particularly for cities like Montreal where the large portion of buildings were constructed in the mid 20th century which would be under higher risk of deterioration and damage due to future WDR exposure levels (Fig A.8). Moreover, the findings of the research help identify the increased risk of WDR and moisture related problems, and are essential for the development of design standards that ensure long-term durability of building façades.

4.2 Limitation and future research

There are a few limitations to this research that need to be addressed in future work. The relatively coarse spatial resolution of the GEM simulations (around 50 km) limits its ability to account for the factors that affect wind speed and direction, such as urban regions and realistic topography among the other factors. Therefore, high-resolution simulations (i.e. Resolution finer than 4 km with 1-minute timestep) should be used to capture WDR-related climatic variables more realistically. Moreover, a five-member ensemble of GEM simulation corresponding to the highest emission scenario (RCP8.5) is used. To better quantify uncertainties, multiple regional climate model (RCM) simulations driven by different global climate models (GCMs) for different greenhouse gas emission scenarios should be implemented.

WDR spell calculations in this research follow the definition given in the ISO Standard 15927-3, considering 96 hours as the minimum drying period separating two consecutive spells on a given façade for masonry walls. Future studies should consider shorter drying periods (i.e. 24hrs, 12hrs and 6hrs) to account for rain penetration through other façade types and openings. Furthermore, the developed WDR risk category maps are based on 3-year return levels of the maximum annual WDR spell loads. The defined thresholds for risk categories are based on the BR262 report approach. However, rain penetration depends on building façade materials and insulation in addition to WDR spell exposure. Thus, an appropriate adjustment to the used thresholds might be required.

Furthermore, future work should focus on developing detailed guidelines for façades design and maintenance procedure for existing buildings. A further investigation in the factors that can reduce WDR exposure (such as overhangs and buildings details) should be conducted to minimize WDR damage. It is also highly recommended to conduct detailed studies for buildings which are susceptible to damage due to increased WDR loads in the future, particularly heritage and traditional buildings. These studies should involve detailed CFD modeling, driven by high resolution RCMs, to better estimate future WDR loads and their spatial and temporal distributions on building façades. Heat, Air, Moisture (HAM) analysis, which are essential to assess the response of building components to these loads, should also be included in these studies using the state-of-art HAM tools.

REFERENCES

Abuku, M., Blocken, B., Nore, K., Thue, J. V., Carmeliet, J., and Roels, S. (2009a). On the validity of numerical wind-driven rain simulation on a rectangular low-rise building under various oblique winds. *Building and Environment, 44*(3), 621-632. doi:https://doi.org/10.1016/j.buildenv.2008.05.003

Abuku, M., Janssen, H., and Roels, S. (2009b). Impact of wind-driven rain on historic brick wall buildings in a moderately cold and humid climate: Numerical analyses of mould growth risk, indoor climate and energy consumption. *Energy and Buildings, 41*(1), 101-110. doi:https://doi.org/10.1016/j.enbuild.2008.07.011

Armstrong, E., Hopcroft, P. O., and Valdes, P. J. (2019). Reassessing the Value of Regional Climate Modeling Using Paleoclimate Simulations. *Geophysical Research Letters, 46*(21), 12464-12475. doi:https://doi.org/10.1029/2019GL085127

ASHRAE, (2009). Standard 160-criteria for moisture control design analysis in buildings. ASHRAE.

Blocken, B., Abuku, M., Nore, K., Briggen, P. M., Schellen, H. L., Thue, J. V., . . . Carmeliet, J. (2011). Intercomparison of wind-driven rain deposition models based on two case studies with full-scale measurements. *Journal of Wind Engineering and Industrial Aerodynamics, 99*(4), 448-459. doi:https://doi.org/10.1016/j.jweia.2010.11.004

Blocken, B., and Carmeliet, J. (2000a). Driving Rain on Building Envelopes- I. Numerical Estimation and Full-Scale Experimental Verification. *Journal of Thermal Envelope and Building Science, 24*(1), 61-85. doi:10.1177/109719630002400104

Blocken, B., and Carmeliet, J. (2000b). Driving Rain on Building Envelopes— II. Representative Experimental Data for Driving Rain Estimation. *Journal of Thermal Envelope and Building Science, 24*(2), 89-110. doi:10.1106/EGXC-T4CL-E8VN-9JRL

Blocken, B., and Carmeliet, J. (2004). A review of wind-driven rain research in building science. *Journal of Wind Engineering and Industrial Aerodynamics, 92*, 1079-1130. doi:10.1016/j.jweia.2004.06.003

Blocken, B., and Carmeliet, J. (2005). High-resolution wind-driven rain measurements on a low-rise building—experimental data for model development and model validation. *Journal of Wind Engineering and Industrial Aerodynamics, 93*(12), 905-928. doi:https://doi.org/10.1016/j.jweia.2005.09.004

Blocken, B., and Carmeliet, J. (2006a). The influence of the wind-blocking effect by a building on its wind-driven rain exposure. *Journal of Wind Engineering and Industrial Aerodynamics, 94*, 101-127. doi:10.1016/j.jweia.2005.11.001

Blocken, B., and Carmeliet, J. (2006b). On the accuracy of wind-driven rain measurements on buildings. *Building and Environment, 41*(12), 1798-1810. doi:https://doi.org/10.1016/j.buildenv.2005.07.022

Blocken, B., and Carmeliet, J. (2007). Validation of CFD simulations of wind-driven rain on a low-rise building facade. *Building and Environment, 42*(7), 2530-2548. doi:https://doi.org/10.1016/j.buildenv.2006.07.032

Blocken, B., and Carmeliet, J. (2012). A simplified numerical model for rainwater runoff on building facades: Possibilities and limitations. *Building and Environment, 53*, 59-73. doi:https://doi.org/10.1016/j.buildenv.2012.01.010

Blocken, B., Derome, D., and Carmeliet, J. (2013). Rainwater runoff from building facades: A review. *Building and Environment, 60*, 339-361. doi:https://doi.org/10.1016/j.buildenv.2012.10.008

Boyd, D. W. (1963). *Driving-Rain Map of Canada*. Retrieved from

Briggen, P. M., Blocken, B., and Schellen, H. L. (2009). Wind-driven rain on the facade of a monumental tower: Numerical simulation, full-scale validation and sensitivity analysis. *Building and Environment, 44*(8), 1675-1690. doi:https://doi.org/10.1016/j.buildenv.2008.11.003

Bush, E., and Lemmen, D. S. editors (2019): *Canada's Changing Climate Report*; Government of Canada, Ottawa, ON. 444 p.

Cacciotti, R. (2020). Brick masonry response to wind driven rain. *Engineering Structures, 204*, 110080. doi:https://doi.org/10.1016/j.engstruct.2019.110080

Choi, E. C. C. (1993). Simulation of wind-driven-rain around a building. *Journal of Wind Engineering and Industrial Aerodynamics, 46-47*, 721-729. doi:https://doi.org/10.1016/0167-6105(93)90342-L

Choi, E. C. C. (1994). Determination of wind-driven-rain intensity on building faces. *Journal of Wind Engineering and Industrial Aerodynamics, 51*(1), 55-69. doi:https://doi.org/10.1016/0167-6105(94)90077-9

Erkal, A., D'Ayala, D., and Sequeira, L. (2012). Assessment of wind-driven rain impact, related surface erosion and surface strength reduction of historic building materials. *Building and Environment, 57*, 336-348. doi:https://doi.org/10.1016/j.buildenv.2012.05.004

Foroushani, S. S. M., Ge, H., and Naylor, D. (2014). Effects of roof overhangs on wind-driven rain wetting of a low-rise cubic building: A numerical study. *Journal of Wind Engineering and Industrial Aerodynamics, 125*, 38-51. doi:https://doi.org/10.1016/j.jweia.2013.10.007

Ge, H., Chiu, V., and Stathopoulos, T. (2017). Effect of overhang on wind-driven rain wetting of facades on a mid-rise building: Field measurements. *Building and Environment, 118*, 234-250. doi:https://doi.org/10.1016/j.buildenv.2017.03.034

Ge, H., and Krpan, R. (2009). Wind-driven rain study in the coastal climate of British Columbia. *British Columbia Institute of Technology*, 1-51.

Giorgi, F. (2019). Thirty Years of Regional Climate Modeling: Where Are We and Where Are We Going next? *Journal of Geophysical Research: Atmospheres, 124*(11), 5696-5723. doi:https://doi.org/10.1029/2018JD030094

Hens, H. (2010). Wind-driven rain: From theory to reality. *Thermal Performance of the Exterior Envelopes of Whole Buildings - 11th International Conference*.

Hogberg, A. B., Kragh, M. K., and Van Mook, F. J. R. (1999). A comparison of driving rain measurements with different gauges. *Proceedings of the Fifth Symposium of Building Physics in the Nordic Countries*.

Hoppestad, S. (1955). Slagregn i Norge (in Norwegian), Norwegian Building Research Institute, rapport Nr. 13, Oslo, 1955.

Huang, S. H., and Li, Q. S. (2010). Numerical simulations of wind-driven rain on building envelopes based on Eulerian multiphase model. *Journal of Wind Engineering and Industrial Aerodynamics, 98*(12), 843-857. doi:https://doi.org/10.1016/j.jweia.2010.08.003

IPCC. (2013). *Climate Change 2013: The Physical Science Basis. Contribution of Working Group I to the Fifth Assessment Report of the Intergovernmental Panel on Climate Change* (T. F. Stocker, D. Qin, G.-K. Plattner, M. Tignor, S. K. Allen, J. Boschung, A. Nauels, Y. Xia, V. Bex, & P. M. Midgley Eds.). Cambridge, United Kingdom and New York, NY, USA: Cambridge University Press.

ISO. (2009). *ISO 15927-3: 2009: Hygrothermal Performance of Buildings - Calculation and Presentation of Climatic Data – Part 3: Calculation of a Driving Rain Index for Vertical Surfaces from Hourly Wind and Rain Data*: International Standards Organisation.

Jeong, D. I., and Sushama, L. (2019). Projected Changes to Mean and Extreme Surface Wind Speeds for North America Based on Regional Climate Model Simulations. *Atmosphere, 10*, 497. doi:10.3390/atmos10090497

Karagiozis, A. N., Salonvaara, M., and Kuenzel, H. (2003). *Influence of wind-driven rain data on hygrothermal performance.* Paper presented at the Proceedings of the Eighth International IBPSA Conference, Eindhoven, the Netherlands

Kubilay, A., Carmeliet, J., and Derome, D. (2017). Computational fluid dynamics simulations of wind-driven rain on a mid-rise residential building with various types of facade details. *Journal of Building Performance Simulation, 10*(2), 125-143. doi:10.1080/19401493.2016.1152304

Kubilay, A., Derome, D., Blocken, B., and Carmeliet, J. (2014a). High-resolution field measurements of wind-driven rain on an array of low-rise cubic buildings. *Building and Environment, 78*, 1-13. doi:https://doi.org/10.1016/j.buildenv.2014.04.004

Kubilay, A., Derome, D., Blocken, B., and Carmeliet, J. (2014b). Numerical simulations of wind-driven rain on an array of low-rise cubic buildings and validation by field measurements. *Building and Environment, 81*, 283-295. doi:https://doi.org/10.1016/j.buildenv.2014.07.008

Lacy, R. E. (1965). Driving rain maps and the onslaught of rain on buildings. *Proc. of CIB/RILEM Symposium on Moisture Problems in Buildings, Helsinki, 1965*.

Nath, U. K. D., Chiu, V., and Ge, H. (2015). Measurements of Wind-driven Rain on Mid- and High-rise Buildings in three Canadian Regions. *Energy Procedia, 78*, 2512-2517. doi:https://doi.org/10.1016/j.egypro.2015.11.255

Nik, V., Mundt-Petersen, O., Sasic Kalagasidis, A., and Wilde, P. (2015). Future moisture loads for building facades in Sweden: Climate change and wind-driven rain. *Building and Environment, 93, Part 2*, 362-375. doi:10.1016/j.buildenv.2015.07.012

Nore, K., Blocken, B., Jelle, B., Vincent Thue, J., and Carmeliet, J. (2007). A dataset of wind-driven rain measurements on a low-rise test building in Norway. *Building and Environment, 42*, 2150-2165. doi:10.1016/j.buildenv.2006.04.003

Oh, S.-G., and Sushama, L. (2020). Short-duration precipitation extremes over Canada in a warmer climate. *Climate Dynamics, 54*(3), 2493-2509. doi:10.1007/s00382-020-05126-4

Orr, S. A., and Viles, H. A. (2018). Characterisation of building exposure to wind-driven rain in the UK and evaluation of current standards. *Journal of Wind Engineering and Industrial Aerodynamics, 180*, 88-97. doi:10.1016/j.jweia.2018.07.013

Orr, S. A., Young, M., Stelfox, D., Curran, J., and Viles, H. (2018). Wind-driven rain and future risk to built heritage in the United Kingdom: Novel metrics for characterising rain spells. *Science of The Total Environment, 640-641*, 1098-1111. doi:https://doi.org/10.1016/j.scitotenv.2018.05.354

Pakkala, T. A., Lemberg, A.-M., Lahdensivu, J., and Pentti, M. (2016). Climate change effect on wind-driven rain on facades. *Nordic Concrete Research, Publication NO. 54*, 31-49.

Pérez-Bella, J. M., Domínguez-Hernández, J., Rodríguez-Soria, B., del Coz-Díaz, J. J., and Cano-Suñén, E. (2012). Estimation of the exposure of buildings to driving rain in Spain from daily wind and rain data. *Building and Environment, 57*, 259-270. doi:https://doi.org/10.1016/j.buildenv.2012.05.010

Reid, J., and Garvin, S. (2011). *Wind Driven Rain: Assessment of the Need for New Guidance*. (Tech. Rep. A1533015). Building Research Establishment Scotland

Rocha, R., Julien, M., Salcido, S., Guimaraes, A., Smith, S. (2017, Mar 22), Montreal Is 375 Years Old, But How Old Are Its Buildings?, *CBC News*. Retrieved from https://www.cbc.ca/news2/interactives/montreal-375-buildings/

Rummukainen, M. (2010). State-of-the-art with regional climate models. *WIREs Climate Change, 1*(1), 82-96. doi:https://doi.org/10.1002/wcc.8

Rychtáriková, M., and Vargová, A. (2008). Bionics and wind-driven rain on building facades. *Slovak journal of civil engineering, Vol. 4*, Pages 30-40.

Straube, J. (1998). *Moisture Control and Enclosure Wall Systems.* (Ph.D. Thesis), University of Waterloo, Waterloo, Canada.

Straube, J., and Burnett, E. (1997). *Rain Control and Screened Wall Systems Rain Control and Screened Wall Systems*.

Straube, J., and Burnett, E. (2000). *Simplified prediction of driving rain deposition*.

Straube, J., and Schumacher, C. J. (2006). Driving rain loads for Canadian building design, Report for CHMC by University of Waterloo, Ottawa.

Teufel, B., Sushama, L., Huziy, O., Diro, G. T., Jeong, D. I., Winger, K., . . . Nguyen, V. T. V. (2019). Investigation of the mechanisms leading to the 2017 Montreal flood. *Climate Dynamics, 52*(7), 4193-4206. doi:10.1007/s00382-018-4375-0

Van den Brande, T., Blocken, B., and Roels, S. (2013). Rain water runoff from porous building facades: Implementation and application of a first-order runoff model coupled to a HAM model. *Building and Environment, 64*, 177-186. doi:https://doi.org/10.1016/j.buildenv.2013.03.014

Zhao, Y., and Sushama, L. (2020). Aircraft Takeoff Performance in a Changing Climate for Canadian Airports. *Atmosphere, 11*(4). doi:10.3390/atmos11040418

APPENDIX

Location	**Climate ID**	**Elevation (m)**	**Latitiude**	**Longitutde**
Inuvik, **NT**	2202570	67.70	68.30 N	133.48 W
WWhitehorse, **YT**	2101300	706.20	60.71 N	135.07 W
Yellowknife, **NW**	2204100	205.70	62.46 N	114.44 W
Vancouver, **BC**	1108447	4.30	49.20 N	123.18 W
Calgary, **AB**	3031093	1084.10	51.11 N	114.02 W
Edmonton, **AB**	3012205	723.30	53.32 N	113.58 W
Regina, **SK**	4016560	577.60	50.43 N	104.67 W
Winnipeg, **MB**	5023222	238.70	49.92 N	97.23 W
Toronto, **ON**	6158733	173.40	43.67 N	79.63 W
Ottawa, **ON**	6106000	114.00	45.32 N	75.67 W
Montreal, **QC**	7025250	36.00	45.50 N	73.62 W
Quebec, **QC**	7016294	74.40	46.80 N	71.38 W
Halifax, **NS**	8202250	145.40	44.88 N	63.50 W
Charlottetown, **PE**	8300300	48.80	46.29 N	63.13 W
St. John's, **NL**	8403506	140.50	47.62 N	52.74 W
Iqaluit, **NU**	2402590	33.50	63.75 N	68.55 W

Table A.1 Description and details of the observation stations used

City	NE Spell	NE Zone	SE Spell	SE Zone	SW Spell	SW Zone	NW Spell	NW Zone
Montreal	49	R2	41	R2	44	R2	24	R1
	71	**R3**	**61**	**R3**	**45**	**R2**	**29**	**R1**
Vancouver	73	R3	207	R4	97	R3	4	R1
	150	**R4**	**386**	**R4**	**140**	**R4**	**5**	**R1**
Toronto	61	R3	91	R3	59	R3	31	R1
	74	**R3**	**100**	**R4**	**64**	**R3**	**33**	**R1**
Edmonton	45	R2	34	R2	10	R1	49	R2
	58	**R3**	**29**	**R1**	**12**	**R1**	**51**	**R2**
Calgary	41	R2	22	R1	8	R1	42	R2
	58	**R3**	**27**	**R1**	**8**	**R1**	**61**	**R3**
Ottawa	40	R2	44	R2	35	R2	15	R1
	54	**R2**	**68**	**R3**	**39**	**R2**	**19**	**R1**
Regina	60	R3	44	R2	10	R1	24	R1
	84	**R3**	**49**	**R2**	**13**	**R1**	**42**	**R2**
Quebec	37	R2	46	R2	41	R2	14	R1
	50	**R2**	**71**	**R3**	**46**	**R2**	**20**	**R1**
Winnipeg	55	R2	36	R2	14	R1	32	R1
	67	**R3**	**46**	**R2**	**18**	**R1**	**38**	**R2**
Halifax	68	R3	121	R4	94	R3	24	R1
	115	**R4**	**146**	**R4**	**126**	**R4**	**36**	**R2**
Charlottetown	98	R3	92	R3	66	R3	55	R2
	162	**R4**	**127**	**R4**	**77**	**R3**	**68**	**R3**
St john’s	92	R3	105	R4	112	R4	42	R2
	167	**R4**	**163**	**R4**	**114**	**R4**	**45**	**R2**
Whitehorse	5	R1	4	R1	7	R1	9	R1
	9	**R1**	**11**	**R1**	**10**	**R1**	**11**	**R1**
Yellowknife	44	R2	31	R1	13	R1	18	R1
	42	**R2**	**46**	**R2**	**14**	**R1**	**23**	**R1**
Inuvik	20	R1	4	R1	6	R1	31	R1
	28	**R1**	**7**	**R1**	**10**	**R1**	**41**	**R2**
Iqaluit	37	R2	51	R2	29	R1	15	R1
	69	**R3**	**86**	**R3**	**78**	**R3**	**65**	**R3**

Table A.2 The volume of 3-year return level WDR spell (L m-2) deposited on building envelope and the WDR spell exposure zone for 16 Canadian cities for four more façade orientations for the 1981-2010 (Light font) and 2071-2100 (**Bold font**) periods

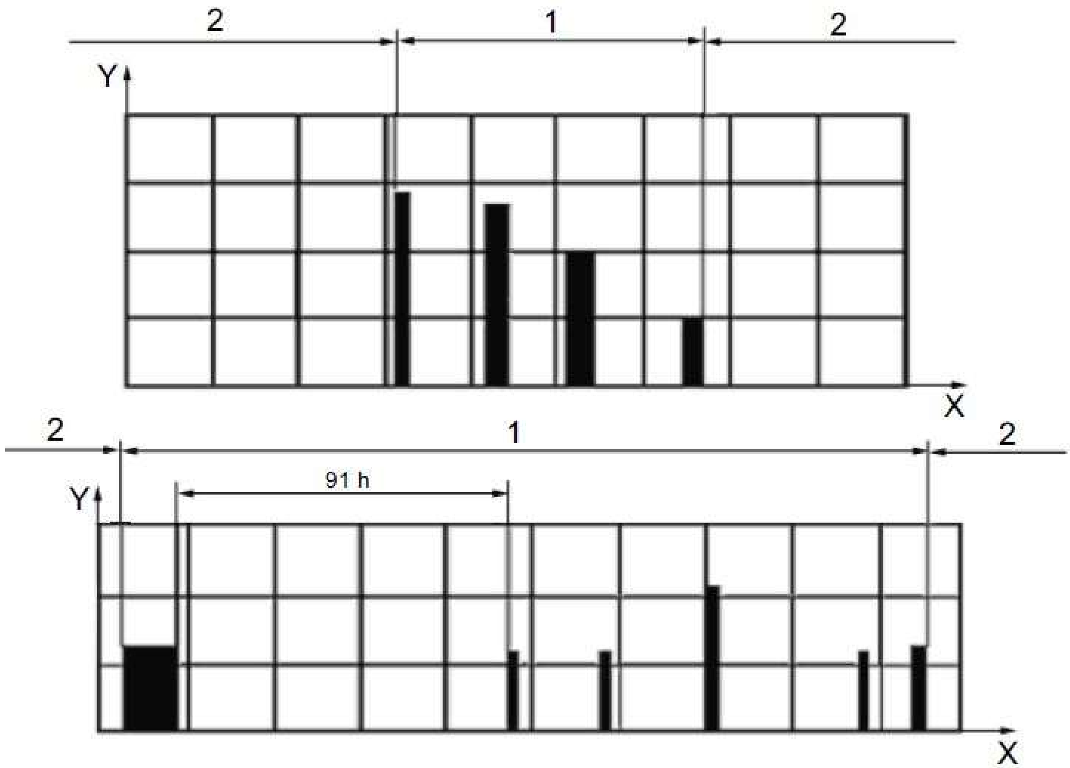

Figure A.1 Schematic representation of defining WDR spells and the period between two spells. X refers to time (days) where each tic represents a half day, Y is input of WDR, (1) period of a spell, and (2) drying period of 96 hrs or more to next spell (ISO, 2009).

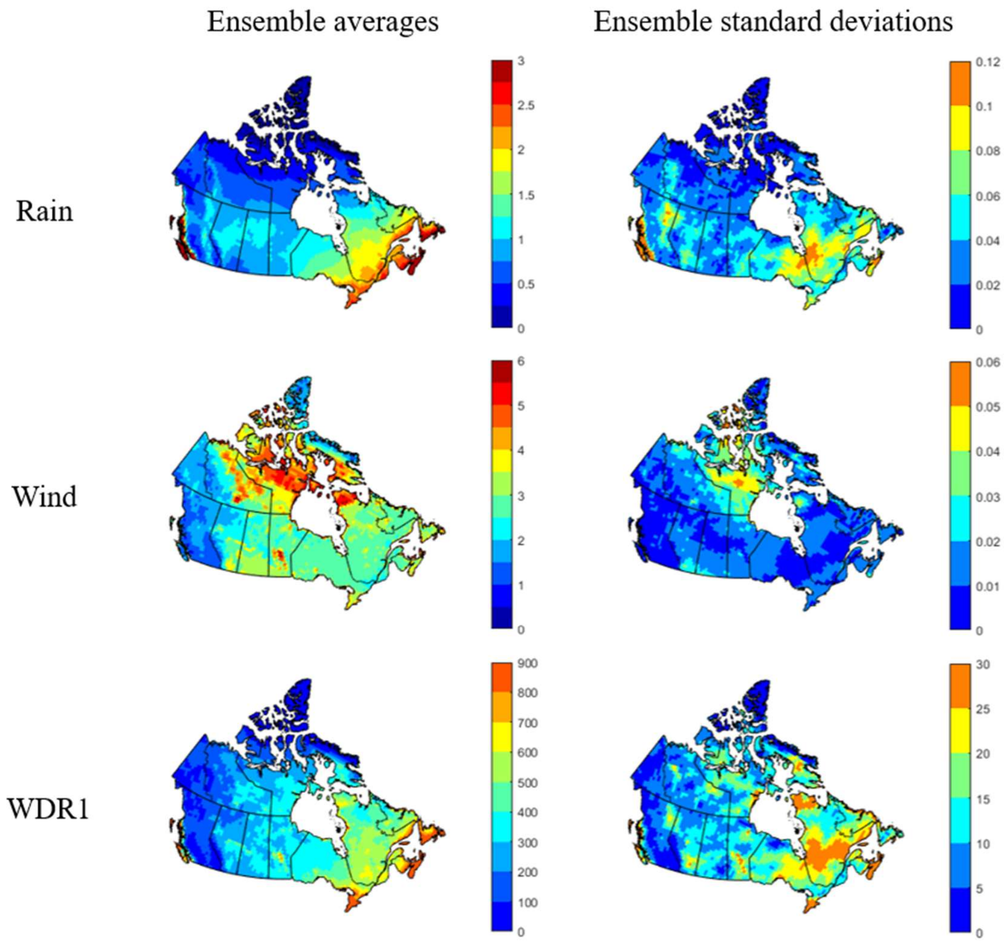

Figure A.2 Ensemble average and standard deviation values of annual mean rainfall, wind speed and WDR1 for the 1981-2010 period.

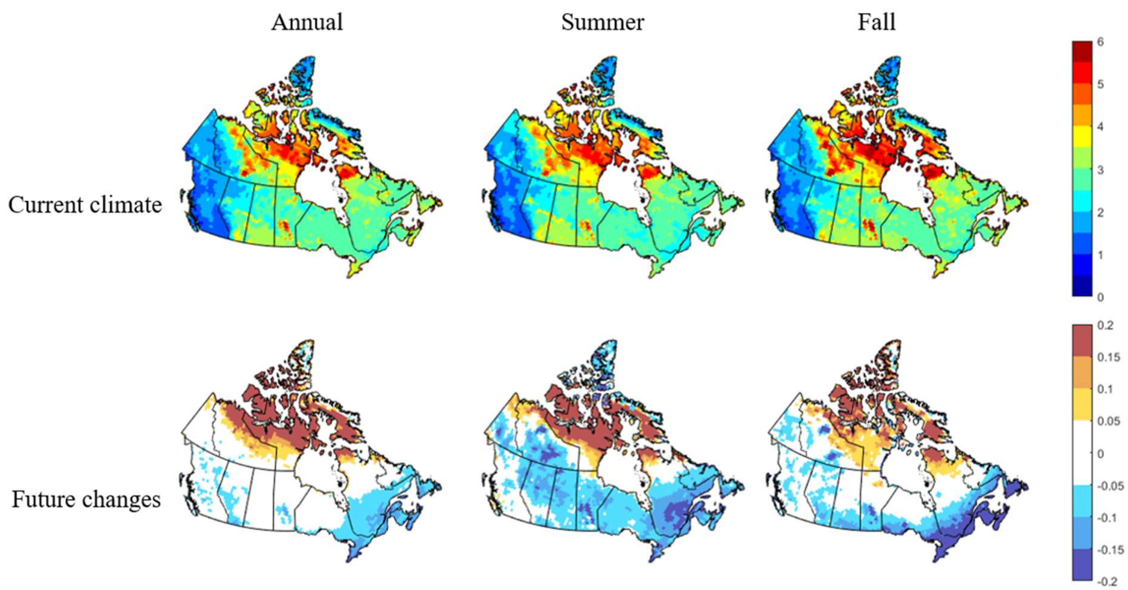

Figure A.3 Projected changes to the annual, summer (JJA) and fall (SON) mean wind speed (m/s) during all-hours obtained for GEM-CanESM2 simulation, for the future 2071-2100 period with respect to the current 1981-2010 period.

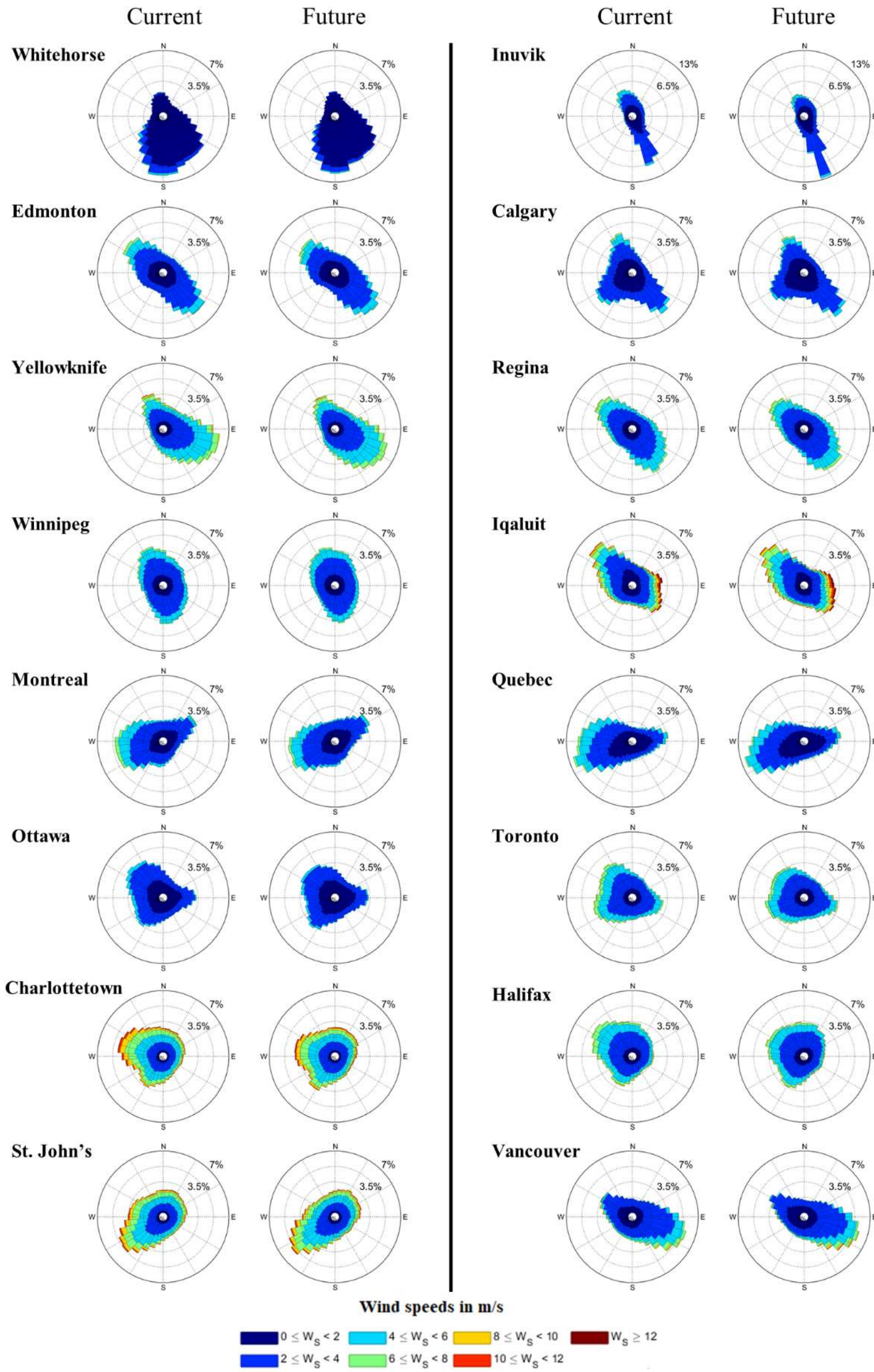

Figure A.4 Directional distributions of wind speeds (m/s) for all hours for 16 Canadian cities derived from GEM-ERAInterim simulation, station observations and ERA5 reanalysis for the 1981-2010 period.

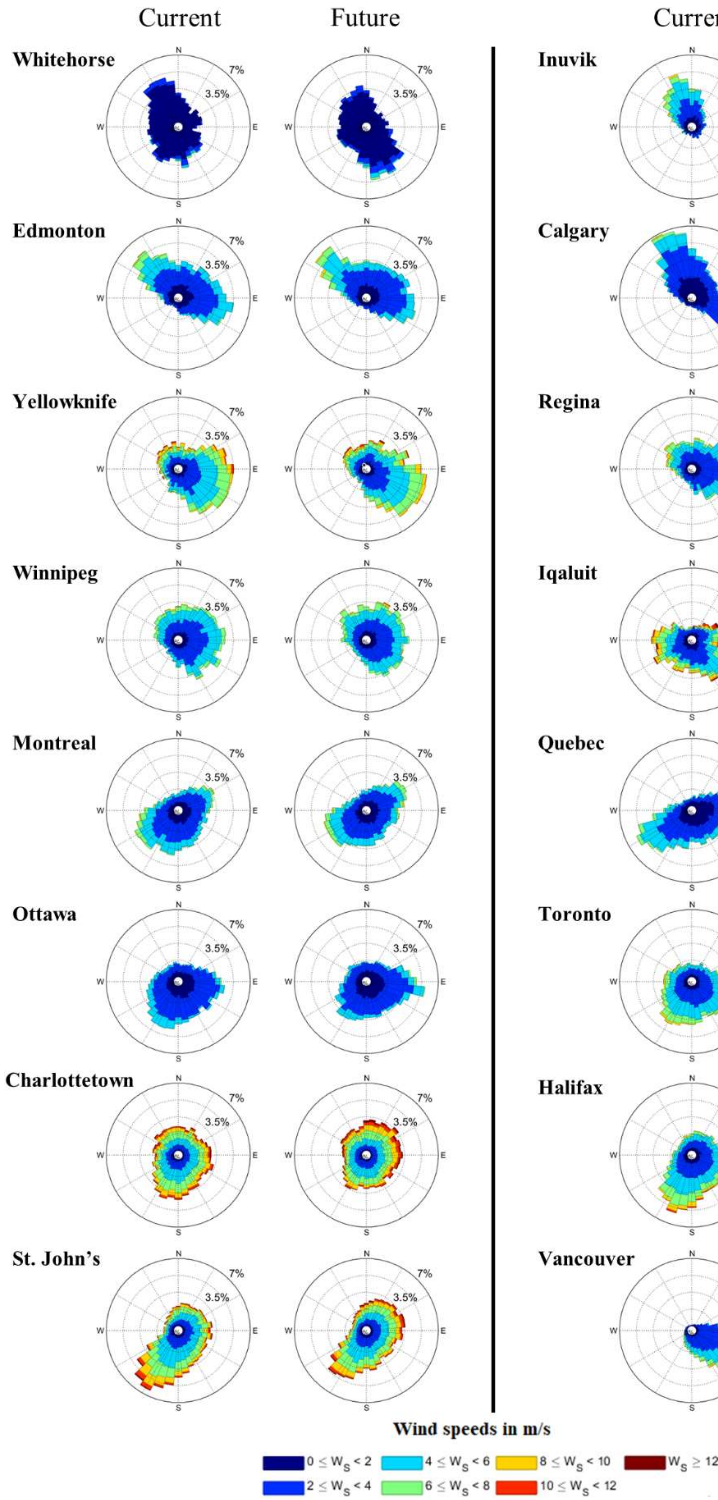

Figure A.5 Directional distributions of wind speeds (m/s) for rainy hours for 16 Canadian cities derived from GEM-ERAInterim simulation, station observations and ERA5 reanalysis for the 1981-2010 period.

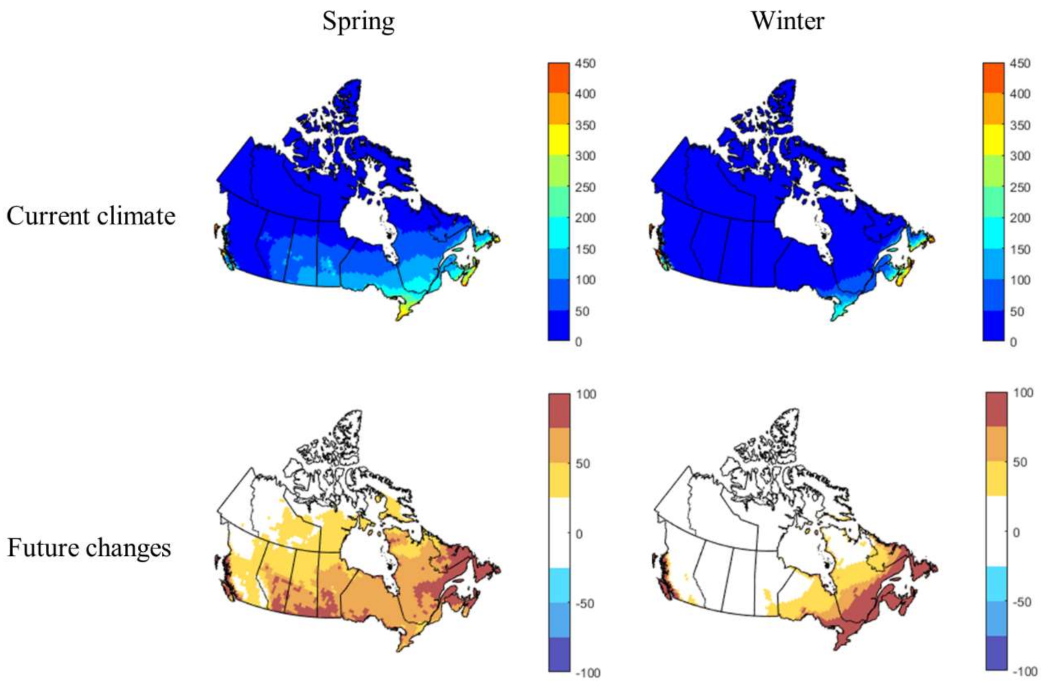

Figure A.6 Projected changes to total annual, spring (MAM) and winter (DJF) WDR loads (mm) obtained from GEM-CanESM2 simulation, for the future 2071-2100 period with respect to the current 1981-2010 period.

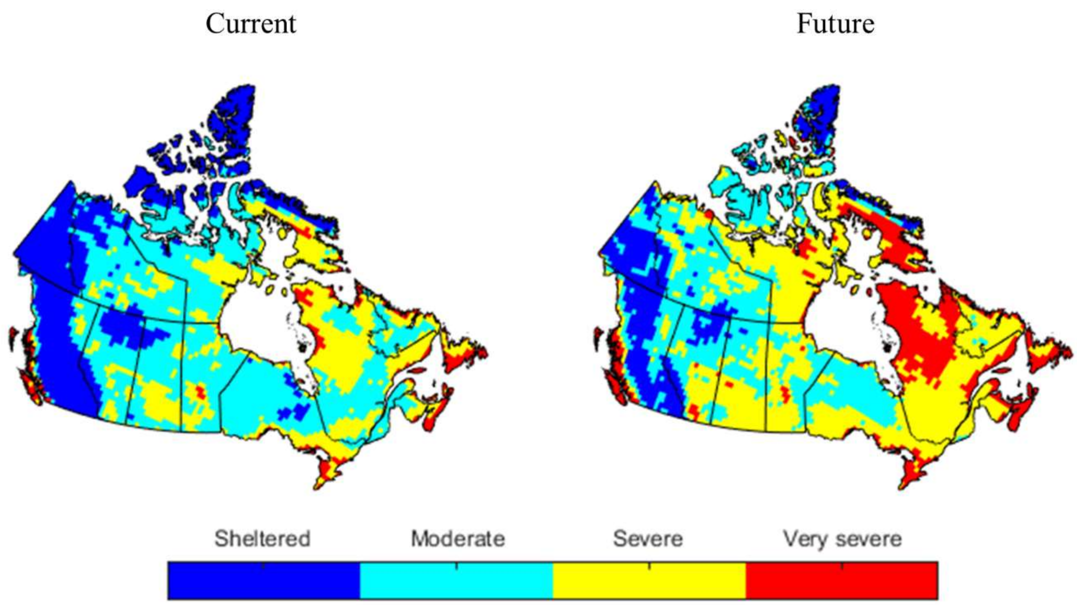

Figure A.7 WDR exposure zones for Canada based on the most critical facade orientation for the 1981-2010 and 2071-2100 periods.

(a) 1600-1930

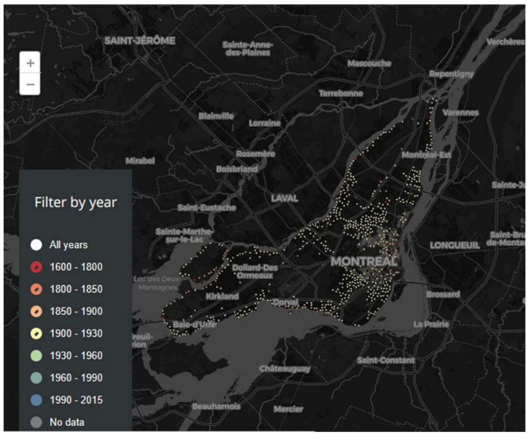

(b) 1930-1960

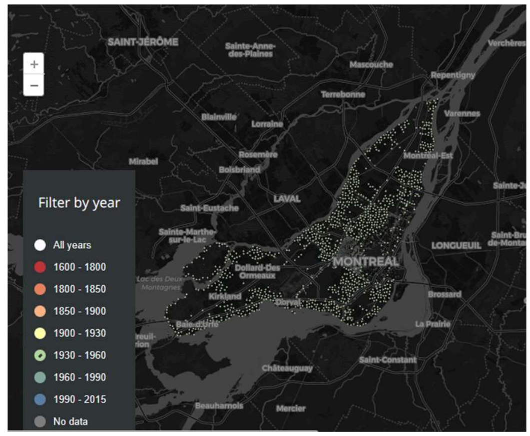

(c) 1960-1990

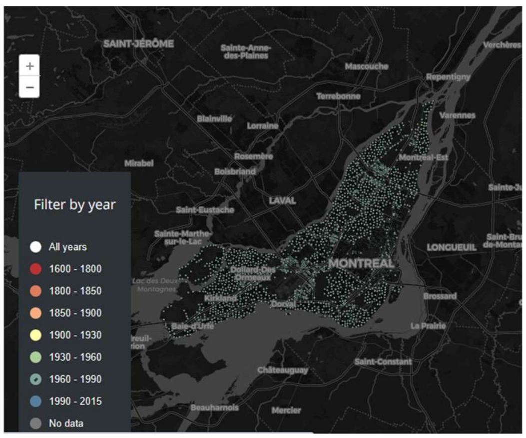

(d) 1990-2015

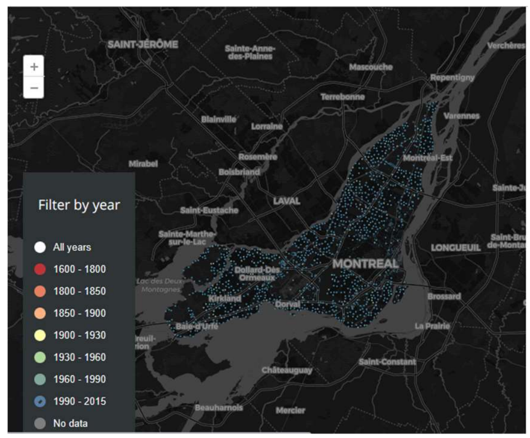

Figure A.8 Classification of buildings in Montreal according to their year of construction; (a) the 1600-1930 period (b) the 1930-1960 period (c) the 1960-1990 period and (d) the 1990-2015 period (Rocha et al., 2017).